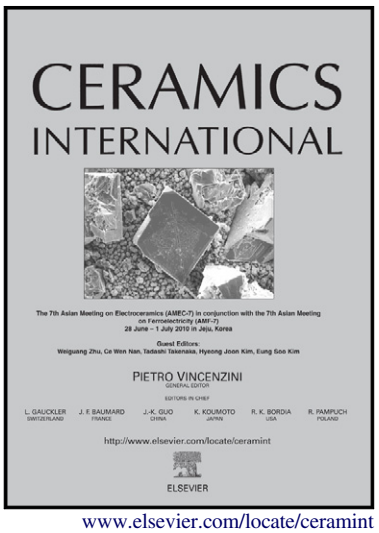

www.elsevier.com/locate/ceramint

Influence of synthesis conditions on formation of core-shell titanate-ferrite particles and processing of composite ceramics

Bojana Mojić-Lanté, Jelena Vukmirović, Konstantinos P. Giannakopoulos, Devendraprakash Gautam, Akos Kukovecz, Vladimir V. Srdić

PII: S0272-8842(14)01461-8
DOI: http://dx.doi.org/10.1016/j.ceramint.2014.09.076
Reference: CERI9195

To appear in: *Ceramics International*

Received date: 24 June 2014
Revised date: 20 August 2014
Accepted date: 12 September 2014

Cite this article as: Bojana Mojić-Lanté, Jelena Vukmirović, Konstantinos P. Giannakopoulos, Devendraprakash Gautam, Akos Kukovecz, Vladimir V. Srdić, Influence of synthesis conditions on formation of core-shell titanate-ferrite particles and processing of composite ceramics, *Ceramics International,* http://dx.doi.org/10.1016/j.ceramint.2014.09.076

Influence of synthesis conditions on formation of core-shell titanate-ferrite particles and processing of composite ceramics

Bojana Mojić-Lanté[1], Jelena Vukmirović[1], Konstantinos P. Giannakopoulos[2], Devendraprakash Gautam[3], Akos Kukovecz[4,5], Vladimir V. Srdić[1]

[1] Department of Materials Engineering, Faculty of Technology, University of Novi Sad, Serbia

[2] Department of Microelectronics, National Centre for Scientific Research "Demokritos", Athens, Greece

[3] Nanoparticle Process Technology, Faculty of Engineering and Center for Nanointegration Duisburg Essen (CeNIDE), University Duisburg-Essen, Duisburg, Germany

[4] Department of Applied and Environmental Chemistry, University of Szeged, Hungary

[5] MTA-SZTE "Lendület" Porous Nanocomposites Research Group, Szeged, Hungary

Corresponding author:

Bojana Mojić-Lanté

Address: Faculty of Technology,
University of Novi Sad,
Bul. Cara Lazara 1,
21000 Novi Sad, Serbia

Phone: +15086657775; +381214853665

Fax: +38121450413

E-mail: bojanamojic@gmail.com

Abstract

Strontium titanate-nickel ferrite ($SrTiO_3$-$NiFe_2O_4$) composite and core-shell particles have been prepared by the combination of sol-gel and co-precipitation route. Modifications of the synthesis procedure (pH value, functionalization of core and shell particles) have been carried out in order to maximize the electrostatic forces between the phases and thus optimize the core-shell morphology of the synthesized powder. It was found that the synthesis pH has considerable influence on the morphology of as-synthesized particles as well as their phase composition. Prepared powders were processed into dense composite ceramics by conventional sintering in air and/or by spark plasma sintering. Particle morphology and thus particle synthesis procedure has proven to have a direct impact on the density, homogeneity and phase composition of the sintered ceramics.

Keywords: *A Powders: chemical preparation; Core-shell particles; D Ferrites; D Titanates; B Composites; B Microstructure-final*

1. Introduction

Over the last few decades, new discoveries in science have promoted interest in the development of new and advanced materials and their investigations on the nanoscale. In addition, the possibility to tailor material properties by changing its structure and composition have brought us into the position to specifically design and fabricate a material for the desired application. A very attractive way to create novel materials is to combine materials with different physical properties in one single structure, thus improving its final functionality.

Core-shell particle structure is one of the possible ways to combine two properties in one nanostructure and thus achieve advanced performances and multifunctionality [1]. One attractive idea, promoting the interest in core-shell particles, is their use as building blocks for bottom-up production of functional nanocomposite ceramics. Recently, Ibanez *et al.* [2] have presented PbTe-PbS core-shell particles as building blocks for highly homogeneous thermoelectric nanocomposite with tuned composition. Hu *et al.* [3] prepared ceramics with excellent microwave dielectric properties starting from core-shell structured $(1\text{-}x)SiO_2$–$xTiO_2$ particles synthesized by sol-gel solvothermal route. Cernea *et al.* [4] argued that Nb doped $BaTiO_3$ coated with SiO_2 could be interesting for application in the composite capacitors. In addition, core-shell particles are recently extensively investigated as a beneficial starting material for multiferroic composite ceramic, where coupling of two ferroic phases (core and shell) results in a new property, magnetoelectric effect (ME). In this case, core-shell structure provides direct and large surface contact of the phases and thus allows significantly higher magnetoelectric effect in comparison to the traditional particulate composites or single-phase multiferroics. Therefore, preparation methods of various ferromagnetic-ferroelectric core-shell structures have been investigated recently. In particular, ferrite-titanate core-shell nanostructures are lately attracting scientific interest due to appropriate individual (magnetostrictive and piezoelectric) properties of the components at room temperature. Synthesis of $BaTiO_3$-γFe_2O_3 [5], $BaTiO_3$-Fe_3O_4 [6], $CoFe_2O_4$-$BaTiO_3$ [7-9], Fe_3O_4-$PbTiO_3$ [9]) and a few studies on processing and characterization of multiferroic composite ceramics from such structures [10-12] have been reported in the literature. However, as stated by Schileo (2013) in the recent review paper addressing the issues of multiferroic composites prepared from core-shell structures [13],

most authors report only the synthesis of core-shell structures, even though the magnetoelectric composites should be prepared in bulk form in order to be used in electronic components. However, both the preparation of the powder and its subsequent densification has a big impact on magnetic, dielectric and magnetoelectric properties of prepared ceramics.

In general, preservation of core-shell structures in processed ceramics is often the issue and perfect core-shell structure does not necessarily lead to core-shell ceramic composites, due to agglomeration, lattice mismatch, different sinterability, interfacial diffusion or phase reaction. In other words, many factors, beside the morphology of the powder, are determining whether the desired characteristics of the final product will be achieved.

This paper addresses the issues of $SrTiO_3$-$NiFe_2O_4$ core-shell nanoparticle synthesis via wet chemical route, and processing of obtained structures into dense ceramics. Strontium titanate ($SrTiO_3$) as an electrostrictive material and incipient ferroelectric, which is known to have favourable and tunable dielectric and ferroelectric properties in solid solution with barium titanate [14, 15] is chosen as a core material, while nickel ferrite ($NiFe_2O_4$) is used as a ferrimagnetic and magnetostrictive shell.

2. Experimental procedure

2.1 Preparation of $SrTiO_3$-$NiFe_2O_4$ particles

Three different nanocrystalline powders consisting of separate strontium titanate and nickel ferrite phases (with composite or core-shell structure) were prepared by the combination of sol-gel and chemical co-precipitation method. Nanocrystalline $SrTiO_3$

nanoparticles were synthesized by sol-gel method, first by controlled hydrolysis of titanium-butoxide ($Ti(OC_4H_9)_4$, Fluka) dissolved in anhydrous ethanol with distilled water (using the water/alkoxide molar ratio of 2 and the titania concentration of 0.5 mol/l). The obtained white titania sol was added to 4 M NaOH aqueous solution under vigorous stirring, to precipitate the titanium hydroxide gel (pH~13). Further reaction of the formed amorphous titanium hydroxide gel with Sr^{2+} ions was performed at 80 °C for 1 h. Strontium nitrate ($Sr(NO_3)_2$, Fluka) was used as precursor for Sr^{2+} ions. Nickel ferrite ($NiFe_2O_4$) nanoparticles were precipitated from an aqueous solution containing Fe^{3+} and Ni^{2+} ions in a molar ratio of 2, obtained from $Fe(NO_3)_3 \cdot 9H_2O$ and $Ni(NO_3)_2 \cdot 6H_2O$. Solution was added to 4 M NaOH and stirred for 1 h at 80 °C.

Depending on the way that STO and NFO particles were mixed, three different samples (with composite or core-shell structure) were prepared. The composite powder *SN13* was obtained by adding the aqueous solution of Fe^{3+} and Ni^{2+} ions to the prepared STO sol, dropwise, at pH~13 and under vigorous stirring at 80 °C for a period of 1 h. In order to promote the mutual (electrostatic) interaction of STO and NFO nanoparticles, and thus achieve core-shell morphology of particles, the sample *SN6* was prepared by addition of aqueous solution with Fe^{3+} and Ni^{2+} ions to the STO dispersion at pH~6. Namely, after synthesis of STO particles at high pH, the powder was washed with distilled water several times. The washed powder was then re-dispersed in distilled water where an aqueous solution with Fe^{3+} and Ni^{2+} ions was added. The sample *SN_F10* was synthesized from previously functionalized STO and NFO nanoparticles. Strontium titanate particles were functionalized with a high charge density cationic polymer, polydiallyldimethylammonium chloride ($(C_8H_{16}NCl)_n$ PDDA, Fluka) by dispersing 500 mg of the washed STO powder in

100 ml of 5 vol.% solution of PDDA in distilled water, and stirred at 70 °C for 30 min to promote the functionalization. The as-functionalized STO powder was subsequently washed and finally dispersed in distilled water at pH~10 with addition of NaOH. NFO particles were functionalized directly after the synthesis, by adding 1 M citric acid ($C_6H_8O_7$, CA) in the solution and stirring for 30 min, maintaining the reaction mixture at 80 °C. The functionalized NFO particles were then added to the suspension of functionalized STO in NaOH and stirred for 30 min at elevated temperature and pH ~10.

All synthesized nanopowders consisting of separate strontium titanate and nickel ferrite phases were prepared with a mass ratio of STO : NFO = 2. The precipitated powders were collected with a centrifuge and washed several times with distilled water to remove sodium ions and finally with absolute ethanol to decrease powder agglomeration by removing free water and replacing the surface hydroxyl with ethoxy groups. Pure STO and NFO powder samples were synthesized for comparative analysis. They were denoted based on their composition: *S* stands for STO and *N* for NFO. In case of composite powders (*SN13*, *SN6* and SN_F10), in addition to the composition, sample denotation indicates the pH value at which the reaction was carried out and whether functionalization ($_F$) of the particles was conducted.

2.2 Preparation of composite ceramics

The prepared powders were consolidated by (i) uniaxial pressing followed by conventional sintering in air, (ii) spark plasma sintering (SPS), or (iii) combination of these two methods. SPS was performed using the equipment FCT HP D5 (FCT Systeme GmbH, Raunstein, Germany). A cylindrical graphite die with 2 cm inner diameter was loaded with

the powder, and a boron nitride coated graphite foil was used to avoid the contact of the powder with the inner surface of the dies. The die was pre-pressed with a pressure of 13 MPa. After that, it was placed in the sintering device and heated by the pulsed electric current with a heating rate of 100 °C/min, with 3 min dwell at maximum temperature (1000 °C, 1100 °C or 1200 °C), and finally cooled down with the same rate to 500 °C and further to room temperature by natural cooling. During the thermal treatment, a uniaxial pressure of 35 MPa was applied to the sample. Conventional sintering in air was performed on pellets uniaxially pressed at 450 MPa, or pre-sintered by means of SPS. Sintering was performed with the heating and cooling rate of 10 °C/min with a 1 h dwell time at maximum temperature, 1000 °C, 1200 °C or 1300 °C.

2.3 Characterization

Particle morphology and composite microstructure were examined by scanning electron microscopy (JEOL, JSM6460LV) and high resolution scanning electron microscopy (JEOL, SEM JSM7500F). Prior to SEM imaging, samples were sputtered with gold. Fresh fractured surface and polished/thermally etched surface (for 30 min at the temperature 50 °C lower than the sintering temperature) of the sintered pellets were examined by SEM. Morphology and crystallinity of particles were additionally investigated by transmission electron microscopy (TEM) (Philips CM 20, Eindhoven, Netherlands) operating at 200 kV, equipped with an energy-dispersive X-ray spectroscopy system (EDS). TEM samples were prepared by drying one drop of ultrasonically dispersed particles on a carbon film supported by a Cu-grid. X-ray diffraction (XRD) of the powders and ceramics was performed using a PANalytical X-ray diffractometer (X'Pert PRO) with a

Ni-filter and Cu$K\alpha$ radiation, operating at 40 mV and 40 mA. The crystallite size of nanopowders was estimated using the Scherrer equation (d=0.9λ/(βcosθ), λ is the wavelength of the X-rays, θ is the scattering angle of the Bragg reflections, β is the full width at half maximum) [16]. Zeta potential of the as-synthesized strontium titanate and nickel ferrite nanoparticles was measured using the M3-PALS method, i.e. the combination of laser Doppler velocimetry and phase analysis light scattering (Zetasizer Nano ZS with MPT-2 Autotitrator, Malvern Instruments, United Kingdom). The density of the sintered pellets was calculated from the geometry and the mass of the sample.

3. Results and discussion

3.1 Morphology and phase composition of STO-NFO particles

STO-NFO particles synthesized in basic conditions

The synthesized STO particles are crystalline, with crystallite size of ~30 nm, as-calculated using Scherrer's equation. XRD (Fig. 1) revealed that besides cubic perovskite $SrTiO_3$, the sample (*S*) contains an insignificant amount of $SrCO_3$ as an impurity phase, which is expected unless great care is taken to ensure that the precursors and the reaction environment are CO_2-free [17-19]. TEM micrographs, presented in Fig. 2a show that primary spherical particles are agglomerated, resulting in a cauliflower particle structure with an average particle size of ~150 nm. On the other hand, the synthesized NFO particles (sample *N*) are very small, having the average size of a few nanometers and very broad XRD peaks characteristic for the ferrite phase (Fig. 1).

In the case of STO-NFO sample prepared at high pH (*SN13*), two phases can be distinguished in TEM micrographs (Figs. 2b, 2c). The fine NFO nanoparticles of about

5 nm are mostly present as free agglomerates of various sizes, but also somewhere attached to the bigger STO particles. Despite the fact that zeta potential investigation showed that both STO and NFO particles are highly negatively charged in the pH range in which the reaction was maintained (Fig. 3), the NFO nanoparticles do attach to the STO surface due to their extremely small particle size leading to a large specific surface area and very high surface energy. Even though XRD of the as-synthesized *SN13* (Fig. 1) shows no peaks characteristic for the ferrite phase, probably due the very small particle size (see XRD pattern of sample *N*), dark field TEM micrograph confirmed that small particles of the shell phase are nanocrystalline (Fig. 2d). In addition, EDS confirmed the presence of all expected elements.

STO-NFO particles synthesized at pH~6

In order to obtain particles with core-shell morphology, guided by the idea that such structures would be more suitable building blocks for homogeneous composite ceramics and would maximize contact between the phases, it was necessary to promote the mutual attraction of STO and NFO particles. Investigation of the zeta potential of the two phases revealed the existence of the "pH window" in pH range of 4.5 to 7, where STO and NFO particles possess opposite surface charge (Fig. 3). One can assume that particle synthesis in this pH range would maximize Coulomb forces between the titanate and ferrite particles, leading to better core coverage and more uniform shell. Indeed, synthesis at pH~6 did result in core-shell morphology, as confirmed by TEM micrograph showing complete coverage of STO particles with NFO shell (Fig. 4a). However, quite nonuniform morphology and thickness of the shell, and even very big ferrite agglomerates attached to the core particles

can also be seen (Fig. 4b). Agglomeration of ferrite nanoparticles occurs due to the van der Waals forces between them and is irreversible, meaning that the energy required to separate two particles, once agglomerated, is very large [20].

Thus, even though synthesis at pH~6 showed to be beneficial in terms of shell formation in comparison to synthesis at pH~13, it proved difficult to maintain the desired phase composition under those reaction conditions. Besides the considerably smaller size of STO crystallites (~17 nm) in comparison to the sample *SN13* (Fig. 1), diffraction pattern confirmed the appearance of the Fe_2O_3 peaks, after calcination at 600 °C for 1 h (Fig. 5). It is known that alkaline conditions are necessary for formation of spinel ferrites, i.e. transformation of metal hydroxides into ferrites [21]. In the case of co-precipitation of ferrite particles at lower pH values, different forms of iron oxides can be formed, unless the ratio of ions is increased [22].

STO-NFO particles synthesized from functionalized particles

In order to obtain core-shell particles with desired composition, functionalization of the particle surface was performed. In this particular case, benefit of particle functionalization is two-fold: (i) firstly, it can provide steric or electrostatic stabilization of small ferrite particles, and in this way prevent them from coming too close to each other and forming big agglomerates due to van der Waals forces; (ii) secondly, it can provide opposite surface charge of STO and NFO at higher pH, promoting the formation of core-shell particles instead of the simple particulate mixture of two phases, and in the same time ensuring the formation of the desired NFO phase.

Zeta potential as a function of pH for the STO and NFO particles after the functionalization with PDDA and CA, respectively, is presented in Fig. 6. Obviously, PDDA acts as a functionalization electrolyte and yields a stable dispersion of STO, providing a positive particle charge due to positively charged ammonium groups. On the other hand, zeta potential of the NFO particles is shifted to more negative values, providing negative particle charge in the whole pH range, and indicating the adsorption of citric acid to the particle surface. This is in good agreement with the literature data, since it is known that citric acid may be adsorbed on the surface of the ferrite nanoparticles by co-ordinating via one or two carboxylate functionalities, leaving at least one carboxylic acid group exposed to the solvent, and thus making the surface negatively charged [23]. As can be seen in Fig. 7, the functionalization of NFO and STO did promote the formation of core-shell particle morphology. Thus, the STO particles are fully covered with a shell of NFO nanoparticles, and continuous nanoparticulate shell is formed. At the same time, no undesired phases could be noticed upon calcination at 600 °C (Fig. 5).

3.2 Microstructure and phase composition of ceramics

Conventional sintering in air

The fracture surface of the sintered pure STO and NFO samples shows that conventional sintering of those powders in air, at 1200 °C for 1 h results in relatively dense ceramics (measured density above 90 % theoretical density, t.d.) with uniform grainy structure (Figs. 8a, 8b). Under the same sintering conditions, the composite powder (*SN13*) densifies to ceramics with higher porosity and considerably lower homogeneity (Fig. 8c).

NFO grains in the micrometer range can be noticed indicating segregation of small particles at such elevated temperatures. Even with the increase of the sintering temperature (1300 °C) result is similar, and further densification is hindered due to the existence of the big ferrite areas which are inducing porosity. This pronounced grain coarsening can be expected, taking into account high surface energy of small NFO particles, and the fact that ferrites have generally better sinterability than titanates.

As expected, the powder with core-shell morphology (*SN6*) densifies in more homogeneous ceramics under the same sintering conditions. As can be seen (Fig. 8d) sample of ~95% t.d. was obtained after sintering at 1200 °C in air for 1 h. In the case of the sample obtained from the functionalized powder (*SN_F10*), contrary to the expectations, significant amount of pores appeared (Fig. 8e). The reason for this was not fully clarified and additional research should be conducted in order to confirm the assumptions. Possibly, the high densification of NFO shell phase hinders the evaporation of CO_2, formed during thermal decomposition of $SrCO_3$ impurities at above 1000 °C [24]. Similar is reported for $BaTiO_3$ ceramics, where decomposition of residual $BaCO_3$ in the samples after pore closure resulted in hindering of densification and formation of pores of 5-15 μm during sintering [25]. Retardation of the pore closures is suggested, to minimize the effect of the residual $BaCO_3$ on the densification. Similarly, core-shell morphology of the functionalized powder (*SN_F10*) might cause the pore closure and "trap" the carbonate residuals at lower temperatures in comparison to other samples.

Only in case of sample *SN13*, XRD confirmed all peaks characteristic for cubic perovskite $SrTiO_3$ and cubic spinel $NiFe_2O_4$, with no additional peaks of $SrCO_3$ or any other secondary phase, indicating that no phase reaction occurred during sintering (Fig. 9).

Diffraction pattern of the sintered sample *SN6* on the other hand, showed no presence of NFO phase, indicating that synthesis at pH~6, even though optimal for preparation of core-shell particles, is not suitable for fabrication of building blocks for STO-NFO composite ceramics. Sintering of the functionalized particles, *SN_F10*, did result in ceramics with both desired phases, but presence of hematite (α-Fe_2O_3) was observed as well. The lower reaction temperature during the particle functionalization probably favoured the formation of thermodynamically stable iron-oxy-hydroxide phases in addition to nickel ferrite [26]. However, it can be mentioned that small amount of impurity phases does not necessarily have a bad impact on the properties of obtained ceramics. Buscaglia *et al.* [27] for example, reported interesting magnetic properties of Fe_2O_3-$BaTiO_3$ core-shell ceramics due to the formation of various barium ferrite phases during sintering or post/annealing.

Spark plasma sintering

Obviously, morphology of as-synthesized nanostructures has a crucial impact on the microstructure and characteristics of the obtained ceramics. However, in this work, preservation of the desired phase composition and avoidance of phase reaction proved to be the factors limiting the possibility to adjust the synthesis procedure and in that way play with the morphology of particles and thus the microstructure of ceramics. In order to further investigate the possibility to achieve ceramics with desired phase composition but also with high density, the powder *SN13* was selected for spark plasma sintering (SPS) method. Due to the very high heating rates, SPS is known to possess clear advantages over conventional sintering methods, like possibility to sinter nanometric powders with very little grain growth [28]. Moreover, there are already some indications in the literature that

SPS treatment may result in favourable ferroelectric and magnetoelectric properties of multiferroic composites, in comparison to conventional sintering techniques [27, 29].

Microstructure of the composite *SN13* sample sintered by SPS at 1000 °C is shown in Fig. 8f. Here, no micrometer sized grains and more homogeneous microstructure than in the case of the samples sintered by conventional sintering (with a measured density of 90.9 % t.d.) can be noticed. XRD pattern (Fig. 9) consists of the characteristic peaks of desirable perovskite and spinel phase without any secondary phase. More dense regions can be observed, probably created in areas with more ferrite phase causing the formation of high temperature spots in SPS. However, XRD patterns of the composites fabricated by SPS at higher temperatures (1100 °C and 1200 °C) (Fig. 9) show that phase decomposition of NFO takes place due to reducing atmosphere in the device, leading to the formation of alloy $NiFe_3$. The reducing action of the SPS environment is known to be enhanced at higher temperature [30] and indeed, with the increase of temperature, decrease of nickel ferrite content in the ceramics can be observed, until finally no peaks characteristic for the nickel ferrite phase are present in the sample sintered at 1200 °C (Fig. 9). SPS employs a pulsed DC current to heat up powder compact by Joule heating. In this process, chemical properties and microstructural characteristics of powder such is grain size or degree of agglomeration will affect the sintering, but as well the electrical conductivity of the material in the die. Accordingly, in the case of the composite materials, higher conductivity of one constituent phase may lead to generation of high-temperature spots in the regions adjacent to the conducting particles, and consequently temperature gradients within the specimen, and therefore the sintering or reactions may be promoted in those spots [30]. Taking into consideration the higher electrical conductivity of $NiFe_2O_4$ in comparison to

$SrTiO_3$, the same fact may be responsible for degradation of ferrite phase and yet no change in the titanate phase.

To promote further densification and in this way achieve better contact between the phases, samples sintered by SPS were subsequently sintered in air. In the case of samples sintered at higher temperatures by SPS (1100 °C and 1200 °C) due to big phase and microstructural changes, phase composition could not be recovered even after re-sintering in air at high temperature. On the other hand, sample sintered at 1000 °C by SPS, in which no phase change occurred, was additionally densified by sintering in air at 1000 °C for 1 h. (Fig. 10) without any phase change (Fig. 9). Thus, the combination of low temperature SPS and low temperature conventional sintering might be proposed as an optimal solution for phase preservation and desired densification process in this type of composite ceramics. Explanation for the effectiveness of that sintering combination could be found in similarity with the well-defined "two-step sintering" described by Chen *et al.* [31, 32].

4. Conclusions

The connection between the wet chemical particle synthesis procedure (i.e. the morphology of titanate-ferite composite particles) and the microstructure and phase composition of composite ceramics obtained from those particles was investigated. It was found that core-shell morphology of the $SrTiO_3$-$NiFe_2O_4$ particles could be obtained by maximizing the electrostatic forces between the two phases, either by adjusting the synthesis pH value between 4.5 and 7 or by functionalization of the core and shell particles with PDDA and CA, respectively. Particles with core-shell morphology can be sintered to dense homogeneous composite ceramics (>95% t.d.) by conventional sintering in air at 1200 °C

for 1 h. The synthesis pH value however, has proven to have an impact on the phase composition of the powder and consequently the sintered composites, since the lower pH value favours formation of iron-oxide rather than nickel ferrite. Spark plasma sintering at and above 1100 °C did not prove suitable for sintering of composite ceramic, since reducing atmosphere in the device induced the decomposition of the nickel ferrite phase. However, the combination of SPS and conventional sintering at low temperatures allowed phase preservation and provided satisfactory densification of the composite powder.

Acknowledgment

The authors gratefully acknowledge the financial support provided by the Ministry of Science of the Republic of Serbia, Project no. III45021. Projects COST MP0904, COST IC1208 and OTKA NN 110676 are also acknowledged.

References

[1] V.V. Srdic, B. Mojic, M. Nikolic, S. Ognjanovic, Recent progress on synthesis of ceramics core/shell nanostructures, Process. Appl. Ceram. 7 (2) (2013) 45–62.

[2] M. Ibanez, R. Zamani, S. Gorsse, J. Fan, S. Ortega, D. Cadavid, J.R. Morante, J. Arbiol, A. Cabot, Core-shell nanoparticles as building blocks for the bottom-up production of functional nanocomposites: PbTe-PbS thermoelectric properties, ACS Nano 7 (3) (2013) 2573–2586.

[3] C. Hu, Y. Liu, P. Liu, W. Zhang, J. Zhu, Microwave dielectric properties of (1-x)SiO_2–xTiO_2 composite ceramics derived from core–shell structured microspheres, Mater. Res. Bull. 53 (2014) 54–57.

[4] M. Cernea, B.S. Vasile, A. Boni, A. Iuga, Synthesis, structural characterization and dielectric properties of Nb doped $BaTiO_3/SiO_2$ core–shell heterostructure, J. Alloys Compd. 587 (2014) 553–559.

[5] S. Mornet, C. Ellissalde, O. Bidault, F. Weill, E. Sellier, O. Nguzen, M. Maglione, Ferroelectric-based nanocomposites: toward multifunctional materials, Chem. Mater. 19 (2007) 987–992.

[6] Y.S. Koo, K.M. Song, N. Hur, J.H. Jung, T.-H. Jang, H.J. Lee, T.Y. Koo, Y.H. Jeong, J.H. Cho, Y.H. Jo, Strain-induced magnetoelectric coupling in $BaTiO_3/Fe_3O_4$ core/shell nanoparticles, Appl. Phys. Lett. 94 (2009) 032903.

[7] V.V. Shvartsman, F. Alawneh, P. Borisov, D. Kozodaev, D.C. Lupascu, Converse magnetoelectric effect in $CoFe_2O_4$–$BaTiO_3$ composites with a core-shell structure, Smart Mater. Struct. 20 (2011) 075006.

[8] K. Raidongia, A. Nag, A. Sundaresan, C.N.R. Rao, Multiferroic and magnetoelectric properties of core-shell $CoFe_2O_4$@$BaTiO_3$ nanocomposites, Appl. Phys. Lett. 97 (6) (2010) 062904-1.

[9] R. Liu, Y. Zhao, R. Huang, Y. Zhao, H. Zhou, Multiferroic ferrite/perovskite oxide core/shell nanostructures, J. Mater. Chem. 20 (2010) 10665-10670.

[10] L.P. Curecheriu, M.T. Buscaglia, V. Buscaglia, L. Mitoseriu, P. Postolache, A. Ianculescu, P. Nanni, Functional properties of $BaTiO_3$–$Ni_{0.5}Zn_{0.5}Fe_2O_4$ magnetoelectric ceramics prepared from powders with core-shell structure, J. Appl. Phys. 107 (2010) 104106.

[11] G.V. Duong, R. Groessinger, R.S. Turtelli, Magnetoelectric properties of $CoFe_2O_4$-$BaTiO_3$ core-shell structure composite, IEEE Trans Magn. 42 (2006) 3611–3613.

[12] V. Corral-Flores, D. Bueno-Baques, D. Carrillo-Flores, J.A. Matutes-Aquino, Enhanced magnetoelectric effect in core-shell particulate composites, J. Appl. Phys. 99 (8) (2006) 08J503.

[13] G. Schileo, Recent developments in ceramic multiferroic composites based on core/shell and other heterostructures obtained by sol-gel routes, Prog. Solid State Chem. 41 (2013) 87–98.

[14] Y. Yu, X. Wang, X. Yao, Dielectric properties of $Ba_{1-x}Sr_xTiO_3$ ceramics prepared by microwave sintering, Ceram. Int. 39 (2013) S335–S339.

[15] B. Wodecka-Dus, A. Lisinska-Czekaj, T. Orkisz, M. Adamczyk, K. Osinska, L. Kozielski, D. Czekaj, The sol-gel synthesis of barium strontium titanate ceramics, Mater. Sci.-Poland 25 (3) (2007) 791–799.

[16] J.I. Langford, A.J.C. Wilson, Scherrer after sixty years: a survey and some new results in the determination of crystallite size, J. Appl. Crystal. 11 (1978) 102–113.

[17] W. Xuewen, Z. Zhiyong, Z. Shuixian, Preparation of nano- crystalline $SrTiO_3$ powder in sol-gel process, Mater. Sci. Eng. B 86 (2001) 29–33.

[18] I. MacLaren, C.B. Ponton, A TEM and HREM study of particle formation during barium titanate synthesis in aqueous solution, J. Euro. Ceram. Soc. 20 (2000) 1267–1275.

[19] V.V. Srdic, R.R. Djenadic, Nanocrystalline titanate powders: Synthesis and mechanisms of perovskite particles formation, J. Optoelectron. Adv. Mater. 7 (2005) 3005–3014.

[20] S.P. Grubin, Magnetic Nanoparticles, first ed. Wiley, Weinheim, 2009.

[21] K. Velmurugana, V.S.K. Venkatachalapathyb, S. Sendhilnathan, Synthesis of nickel zinc iron nanoparticles by coprecipitation technique, Mater. Res. 13 (3) (2010) 299–303.

[22] P. Ren, J. Zhang, H. Deng, Preparation and microstructure of spinel zinc ferrite $ZnFe_2O_4$ by co-precipitation method, J. Wuhan. Univ. Technol. 24 (6) (2009) 927–930.

[23] A. Goodarzi, Y. Sahoo, M.T. Swihart, P.N. Prasad, Aqueous ferrofluid of citric acid coated magnetite particles, Mater. Res. Soc. Symp. Proc. 789 (6) (2004) 6.6.1–6.6.6.

[24] K.H. Stern, High Temperature Properties and Thermal Decomposition of Inorganic Salts with Oxyanions, CRC press, USA, 2001.

[25] B.-K. Yoon, E.-Y. Chin, S.-J.L. Kang, Dedensification during sintering of $BaTiO_3$ caused by the decomposition of residual $BaCO_3$, J. Am. Ceram. Soc. 91 (12) (2008) 4121–4124.

[26] C.H. Chia, S. Zakaria, M. Yusoff, S.C. Goh, C.Y. Haw, Sh. Ahmadi, N.M. Huang, H.N. Lim, Size and crystallinity-dependent magnetic properties of $CoFe_2O_4$ nanocrystals, Ceram. Int. 36 (2010) 605–609.

[27] M.T. Buscaglia, V. Buscaglia, L. Curecheriu, P. Postolache, L. Mitoseriu, A.C. Ianculescu, B.S. Vasile, Z. Zhe, P. Nanni, Fe_2O_3@$BaTiO_3$ core-shell particles as reactive precursors for the preparation of multifunctional composites containing different magnetic phases, Chem. Mater. 22 (2010) 4740–4748.

[28] T. Hungria, J. Galy, A. Castro, Spark plasma sintering as a useful technique to the nanostructuration of piezo-ferroelectric materials, Adv. Eng. Mater. 11 (8) (2009) 615–631.

[29] A. Srinivas, M. Manivel Raja, D. Sivaprahasam, P. Saravanan, Enhanced ferroelectricity and magnetoelectricity in $0.75BaTiO_3$-$0.25BaFe_{12}O_{19}$ by spark plasma sintering, Process. Appl. Ceram. 7 (1) (2013) 29–35.

[30] D.V. Dudina, A.K. Mukherjee, Reactive spark plasma sintering: successes and challenges of nanomaterial synthesis, J. Nanomater. 2013 (2013) 625218.

[31] I.W. Chen, X.H. Wang, Sintering dense nanocrystalline ceramics without final-stage grain growth, Nature 404 (2000) 168–171.

[32] X.H. Wang, X.Y. Deng, H.L. Bai, H. Zhou, W.G. Qu, L.T. Li, I.W. Chen, Two-step sintering of ceramics with constant grain-size, II. $BaTiO_3$ and Ni-Cu-Zn ferrite, J. Am. Ceram. Soc. 89 (2006) 439–443.

Figure captions:

Figure 1. X-ray diffraction pattern of as-synthesized *N*, *S*, *SN13* and *SN6* powders

Figure 2. TEM images of the sample *S* (a), and *SN13* taken in the bright field (b)(c) and dark field (d)

Figure 3. Zeta potential as a function of pH value for $SrTiO_3$ and $NiFe_2O_4$ nanoparticles

Figure 4. TEM images of the sample *SN6*

Figure 5. X-ray diffraction pattern of *SN13*, *SN6* and SN_F10 powders calcined at 600 °C for 1 h

Figure 6. Zeta potential as a function of pH value for $SrTiO_3$ functionalized with PDDA and $NiFe_2O_4$ functionalized with CA

Figure 7. TEM micrographs of SN_F10 synthesized with the functionalized particles

Figure 8. Microstructure (fracture surface) of the samples sintered for 1 h at 1200 °C in air: *S* (a), *N* (b), *SN13* (c), *SN6* (d) and SN_F10 (e); and sintered by SPS at 1000 °C: *SN13* (f)

Figure 9. XRD of composite sample *SN13* densified by conventional sintering in air for 1 h (CS), spark plasma sintering for 3 min (SPS) or combination of the two methods (SPS+CS), at indicated temperatures

Figure 10. Polished (a) and thermally etched (b) surface of the sample *SN13* sintered by the combination of SPS (1000 °C) and conventional sintering (1000 °C)

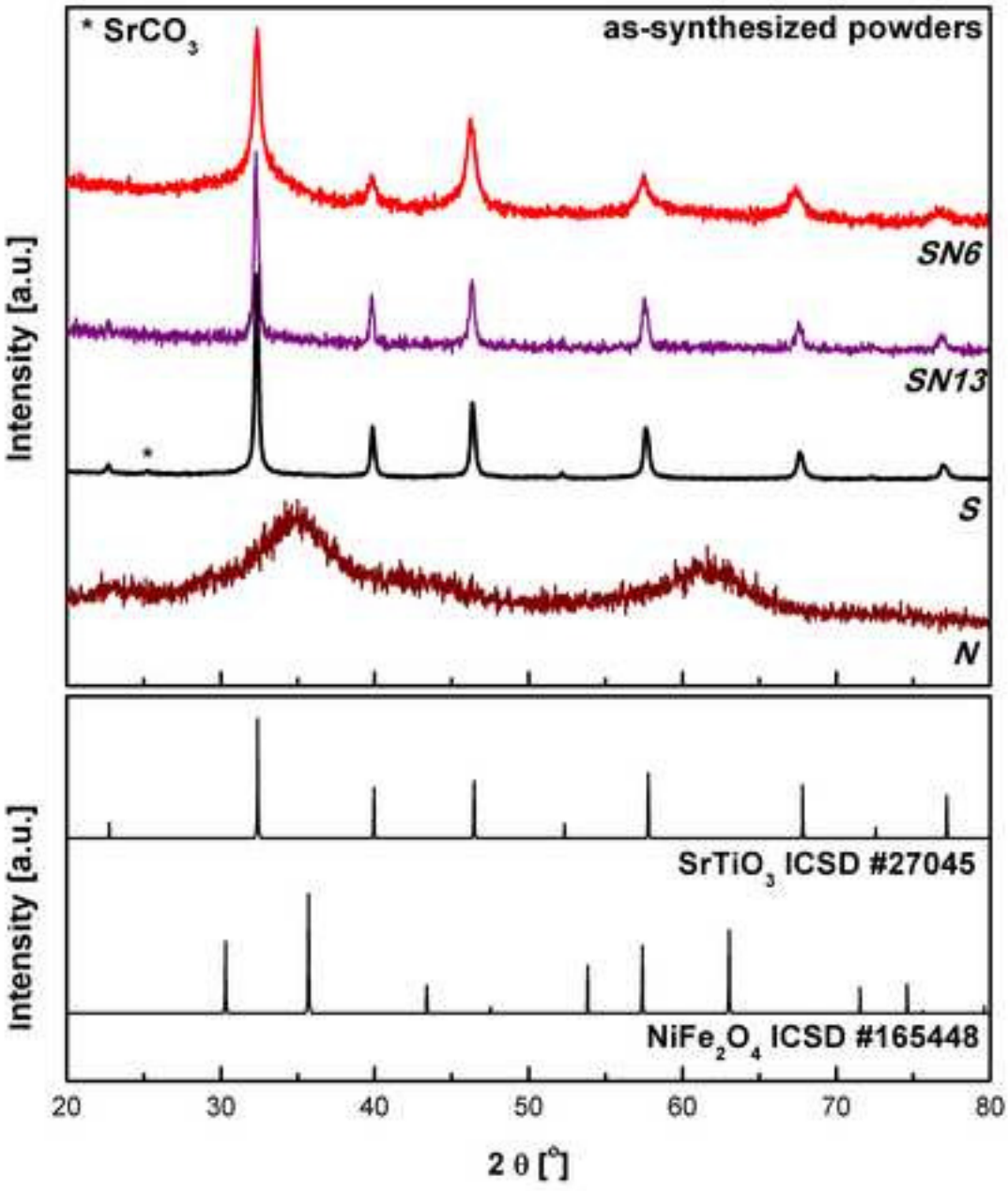

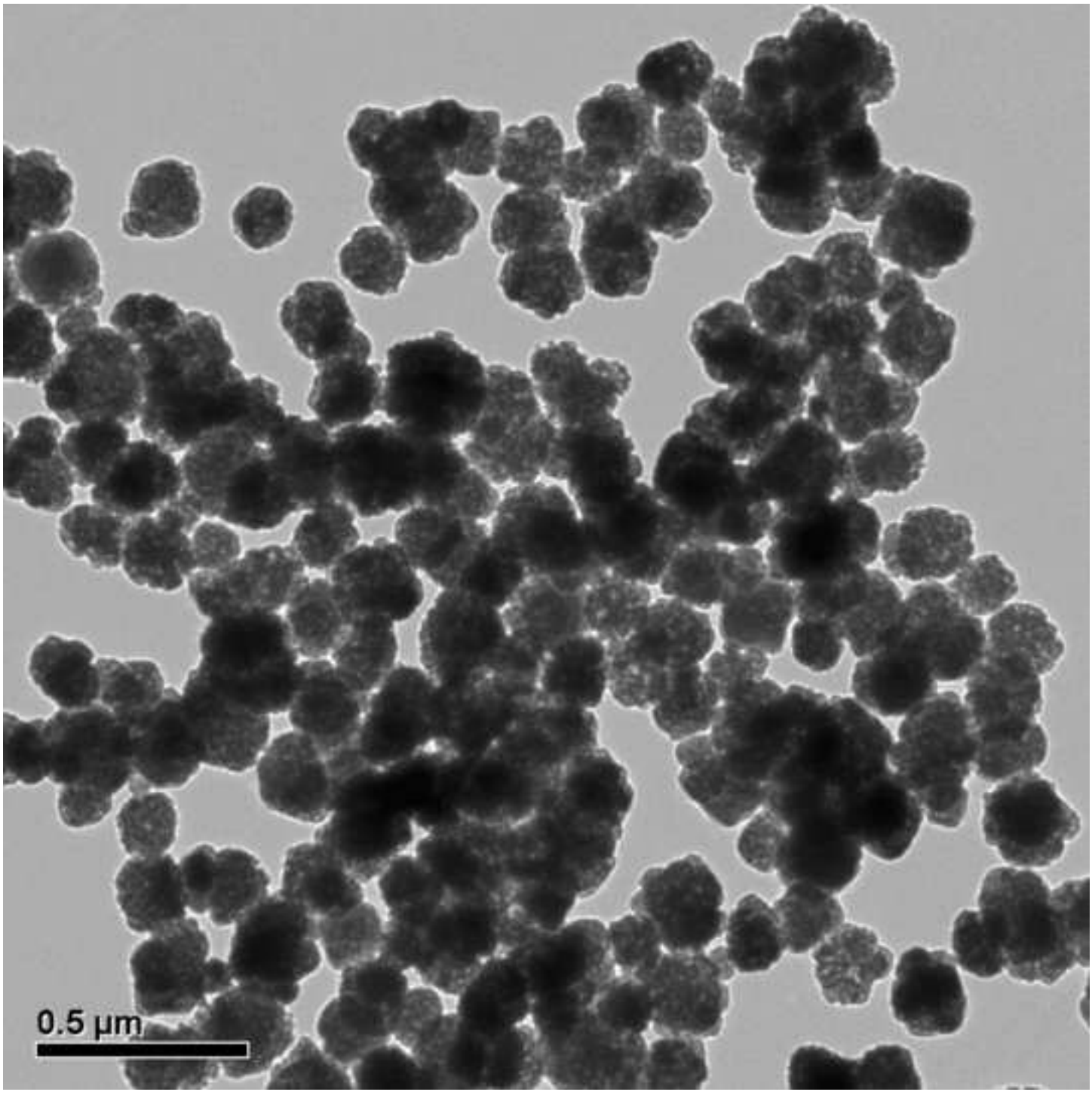

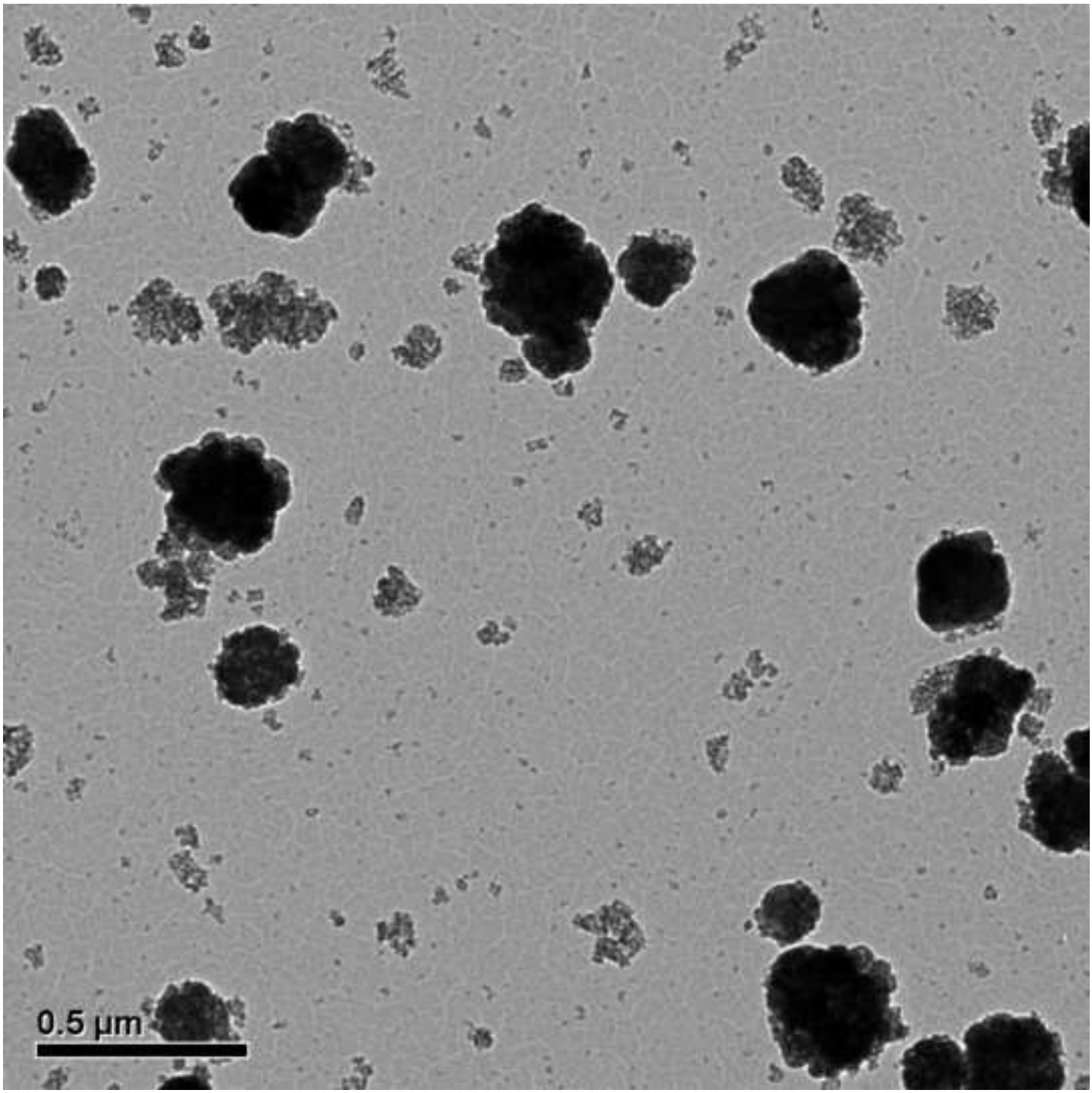

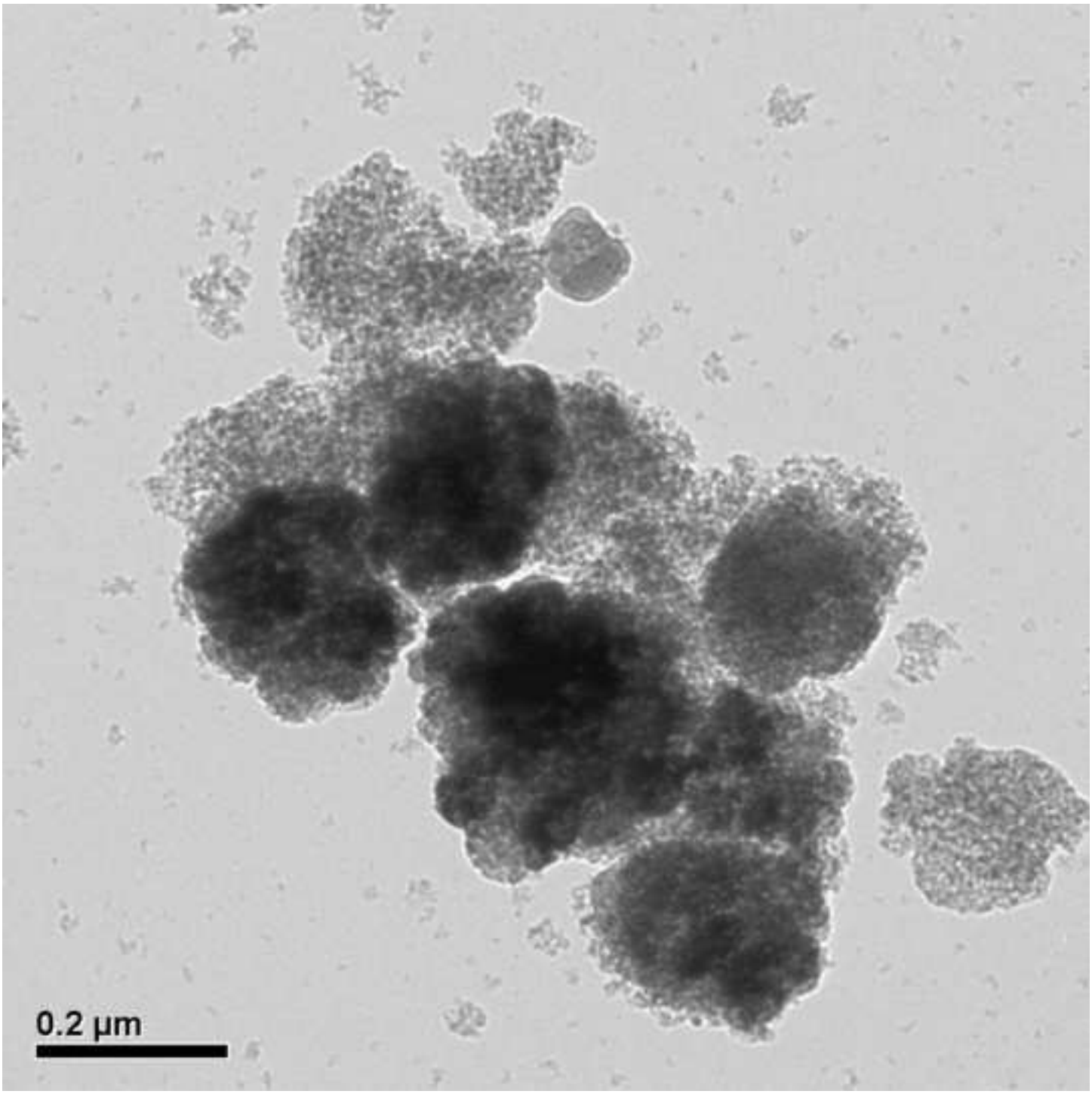

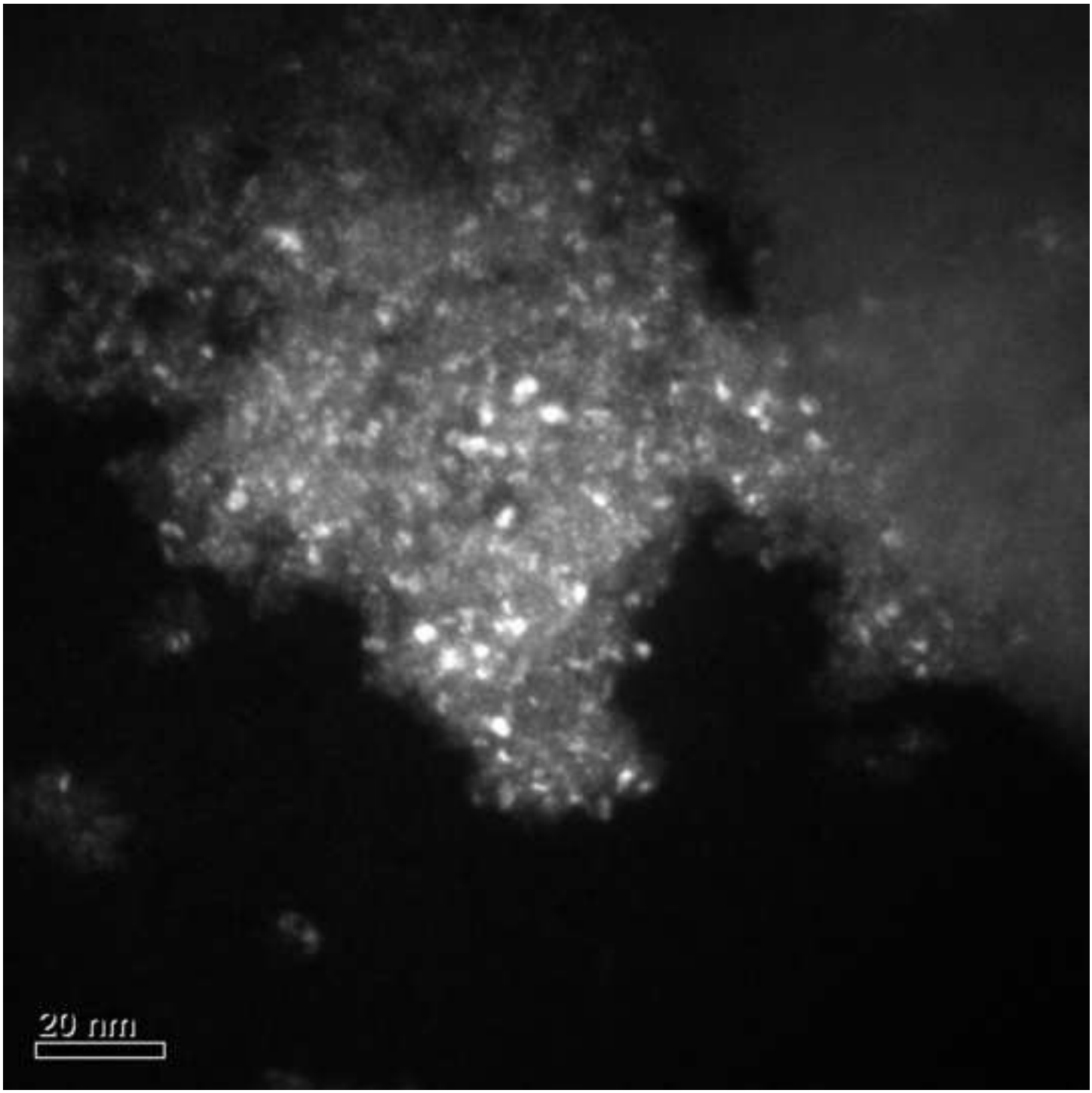

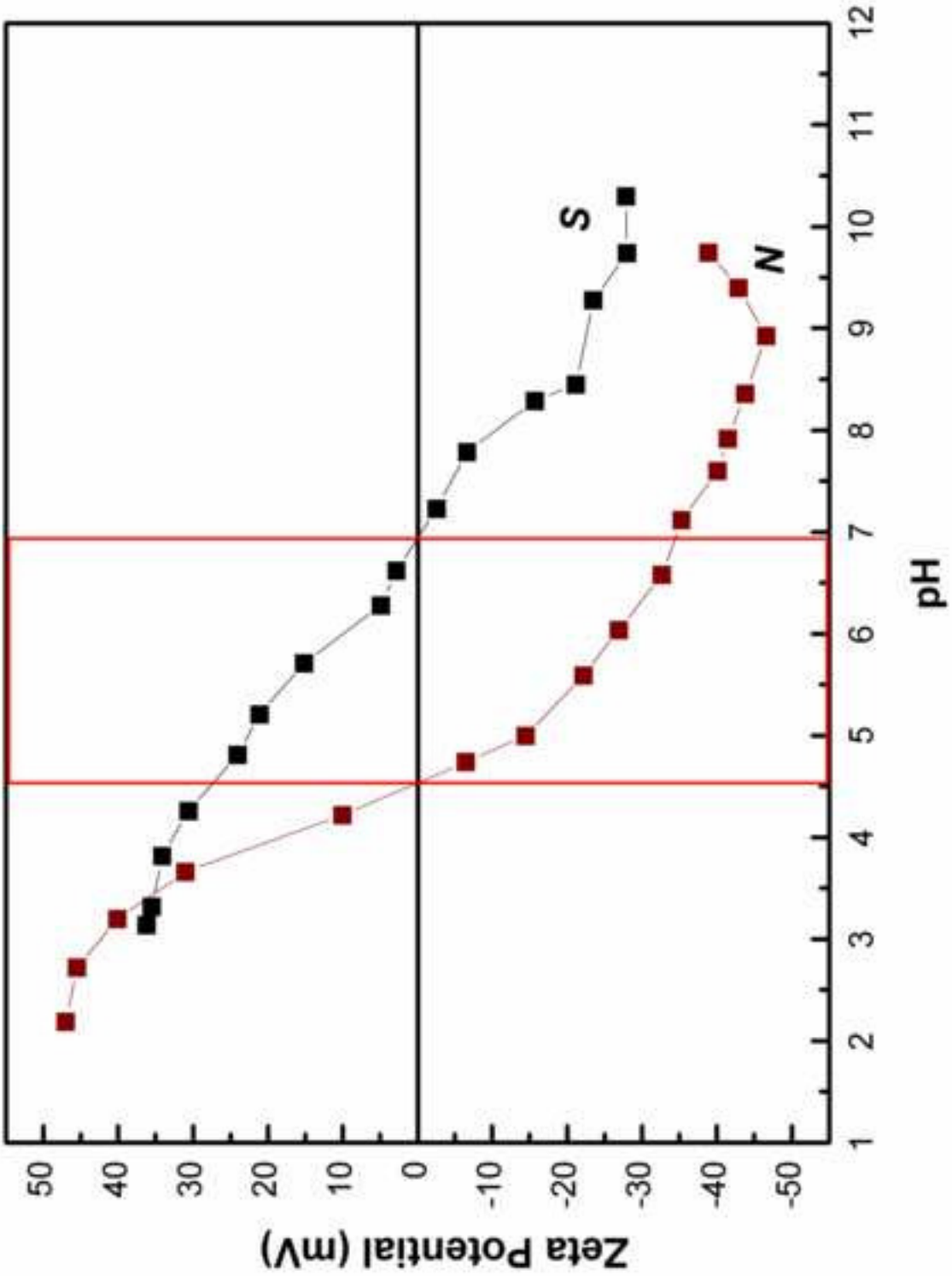
Zeta Potential (mV)
50
40
30
20
10
0
-10
-20
-30
-40
-50
1
2
3
4
5
6
7
8
9
10
11
12
pH
S
N

Figure

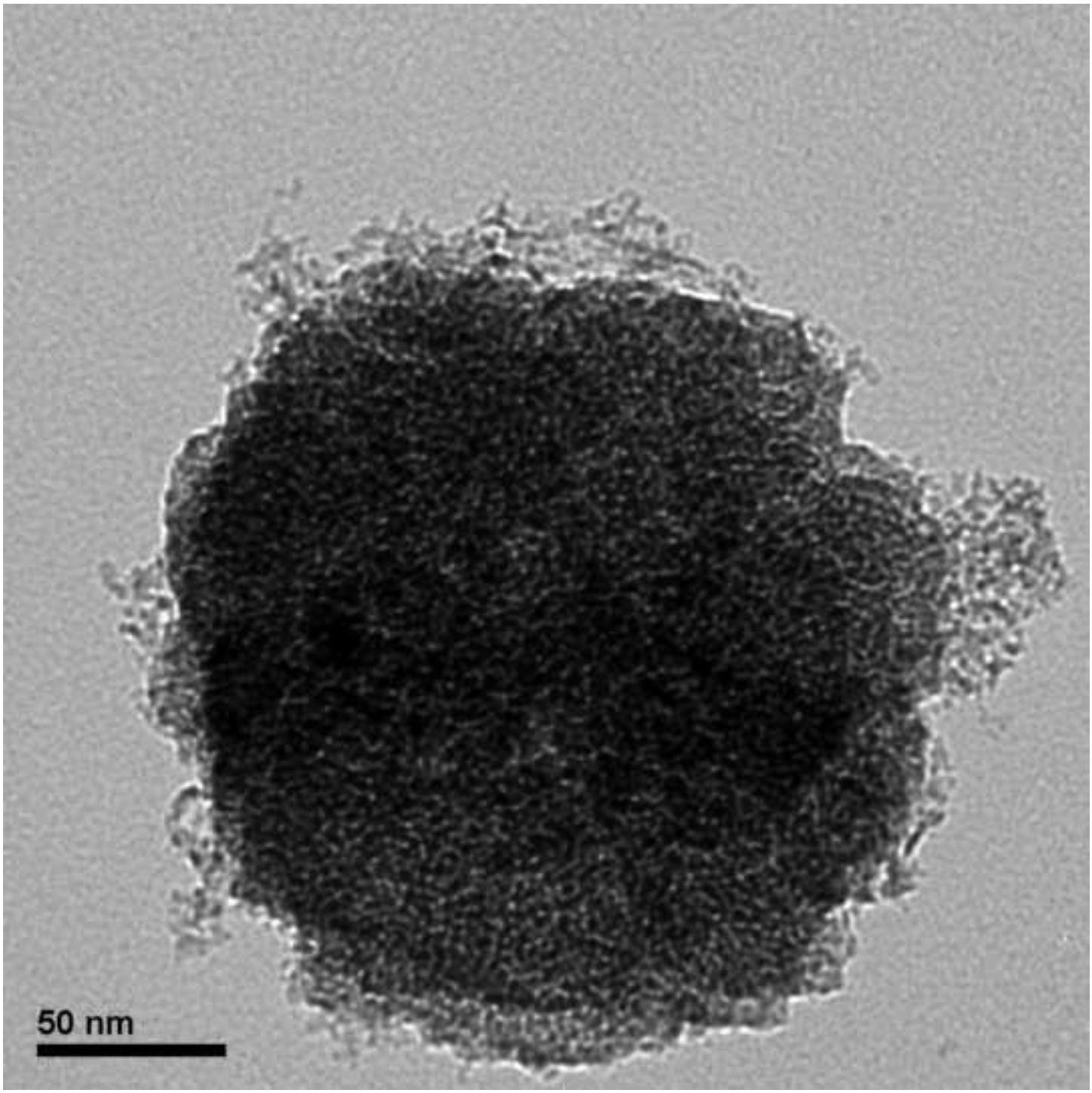

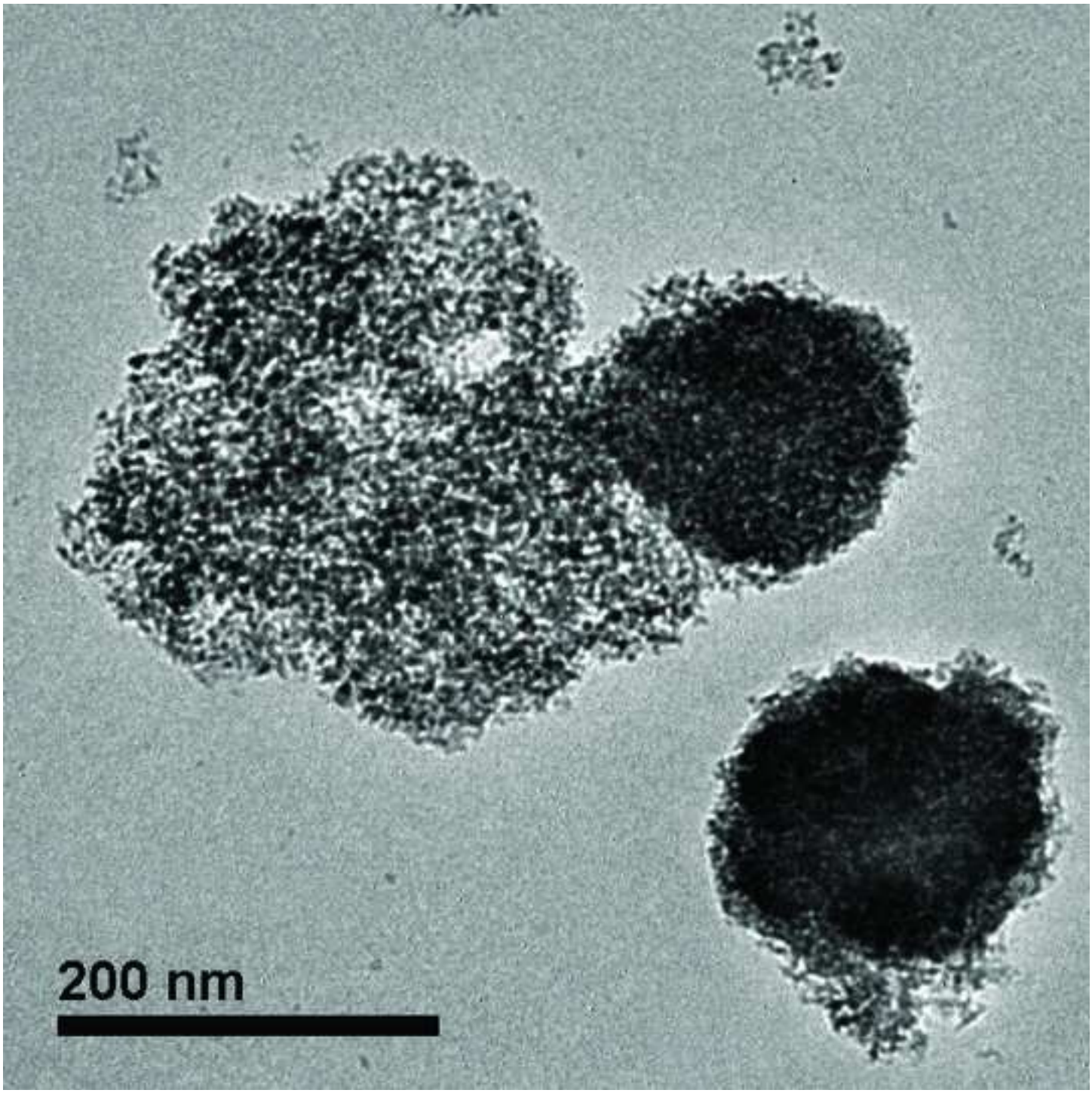

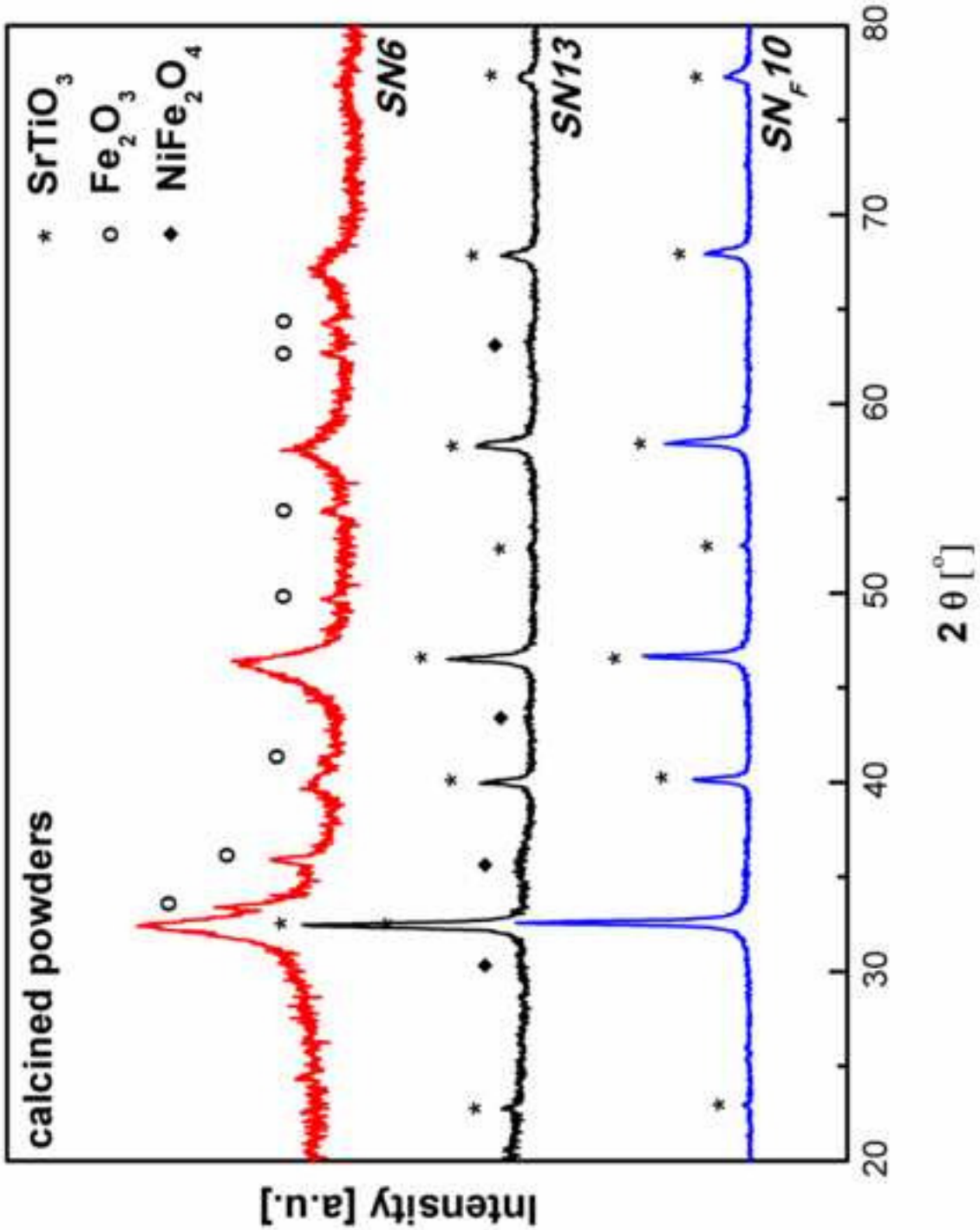
calcined powders
* SrTiO3
o Fe2O3
◆ NiFe2O4
SN6
SN13
SNF10
Intensity [a.u.]
2θ [°]
20
30
40
50
60
70
80

Figure

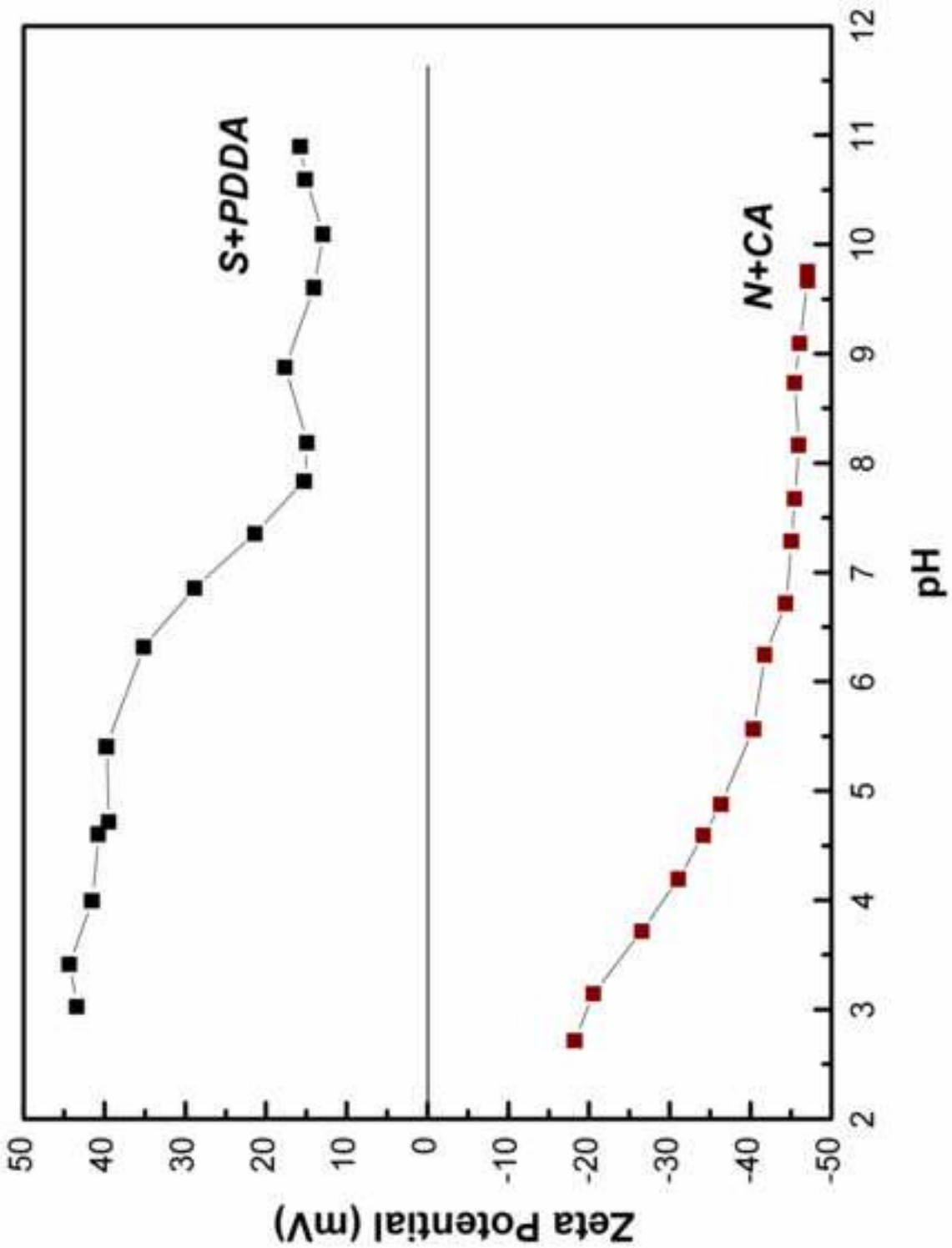
S+PDDA
N+CA
Zeta Potential (mV)
pH
50
40
30
20
10
0
-10
-20
-30
-40
-50
2
3
4
5
6
7
8
9
10
11
12

Figure

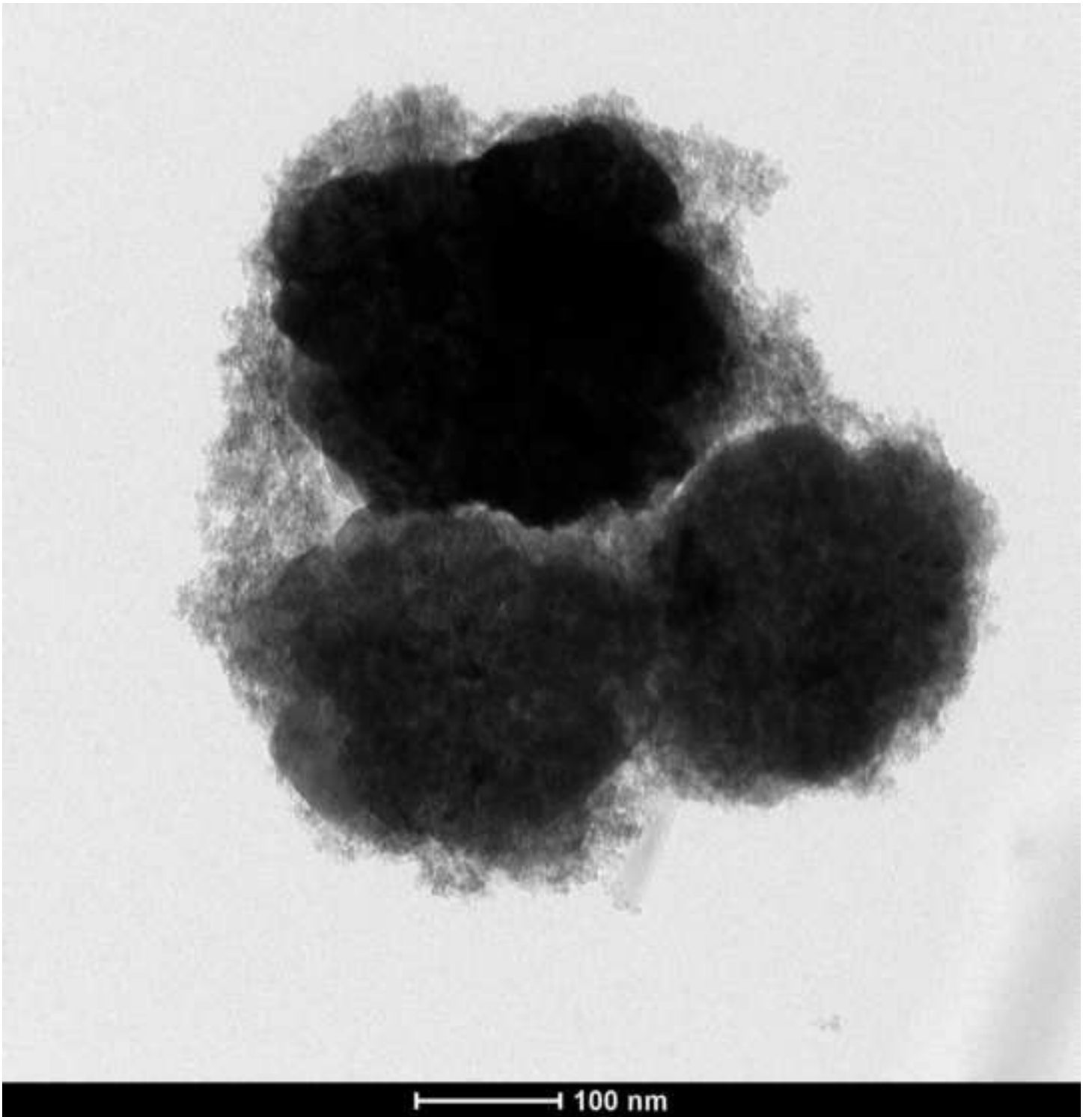

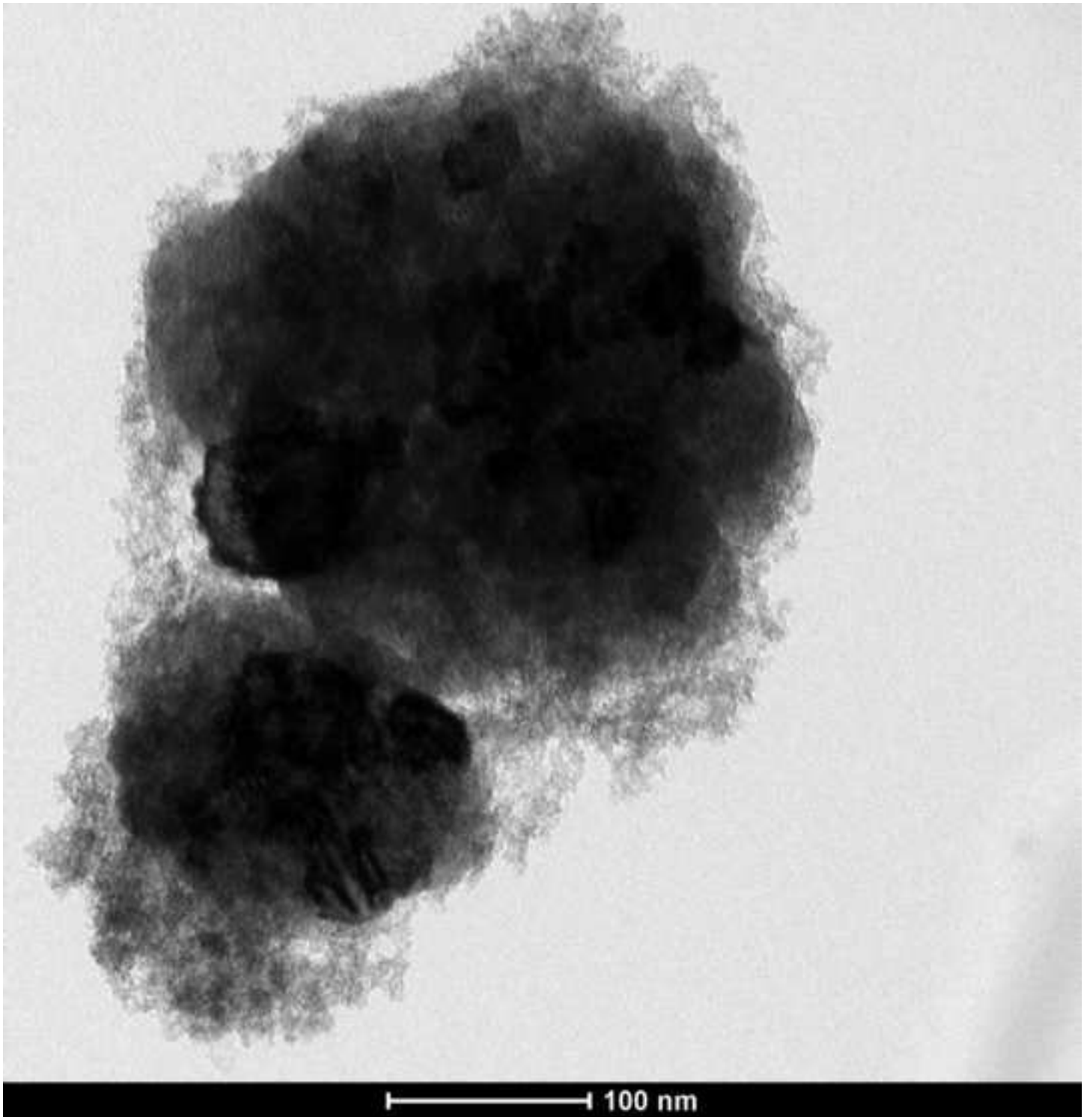

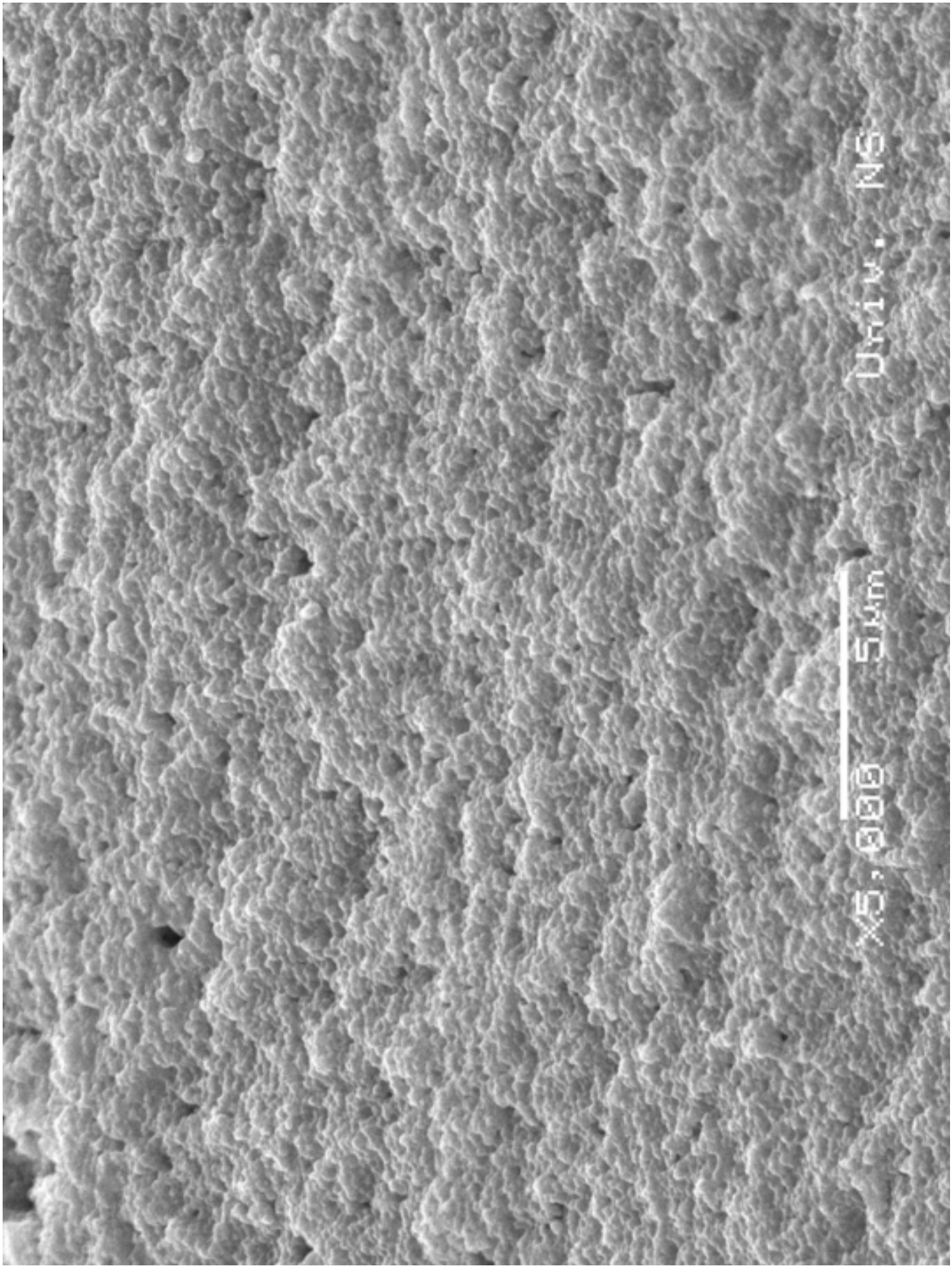

Figure

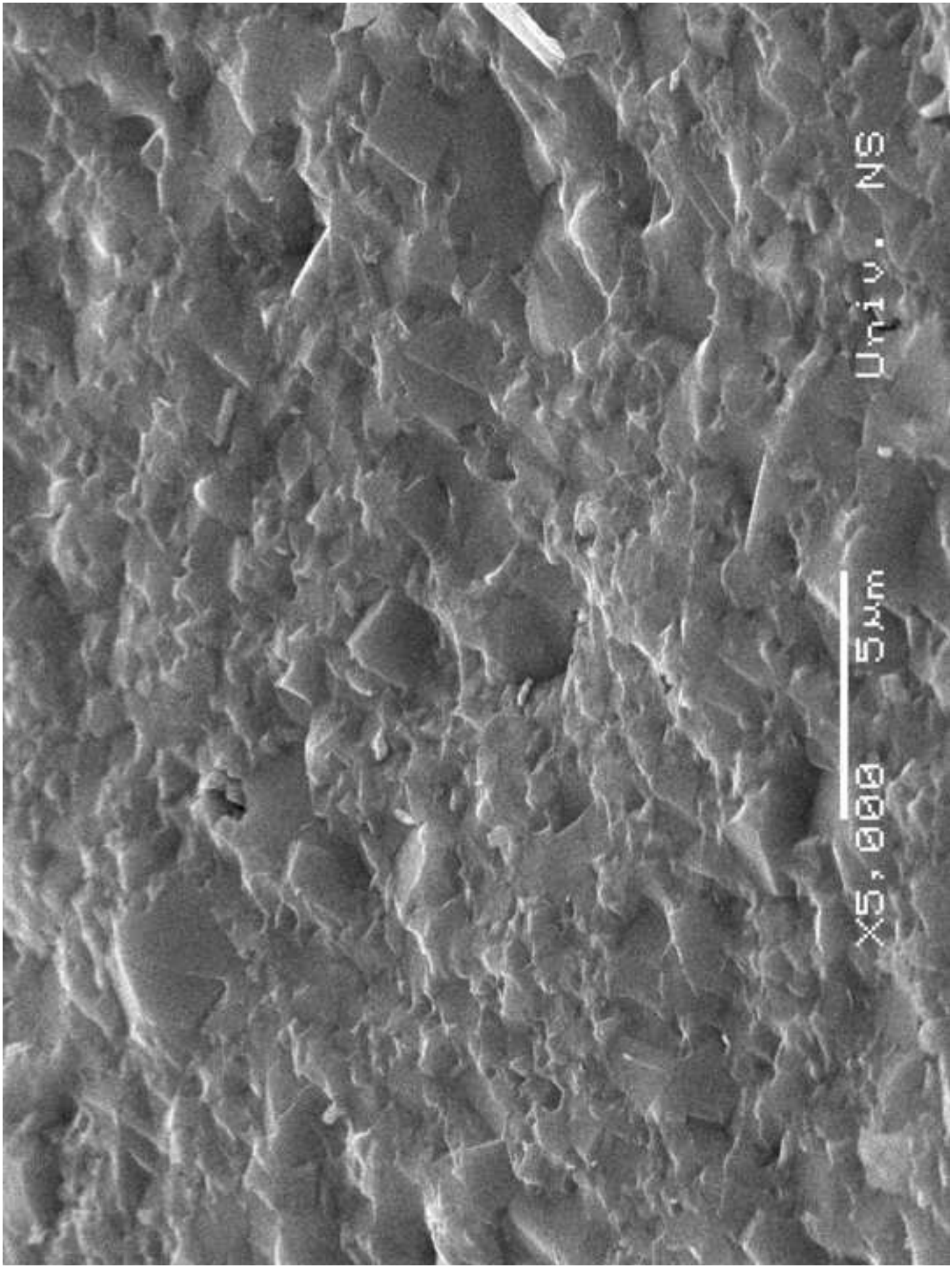

Figure

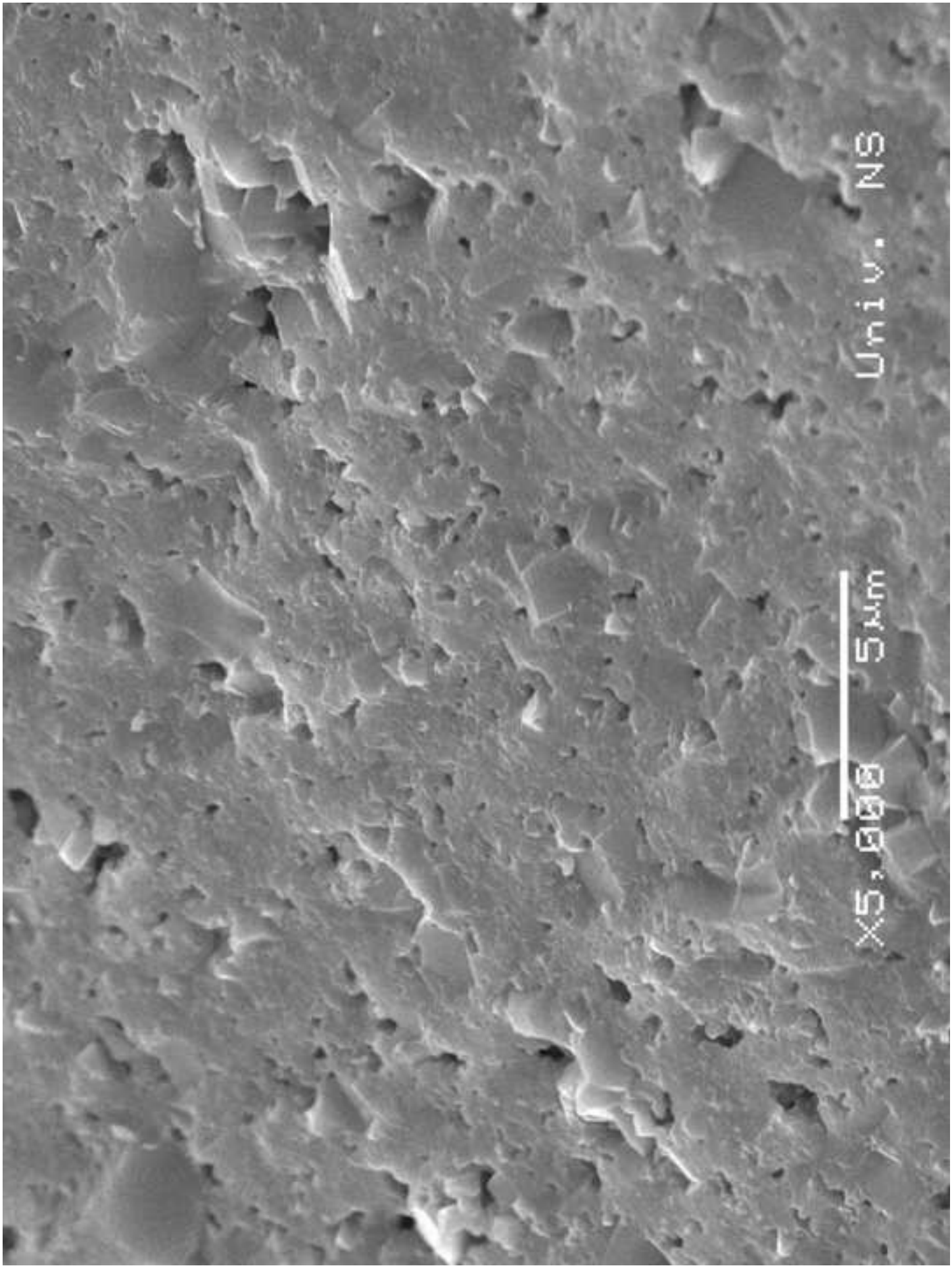

Figure

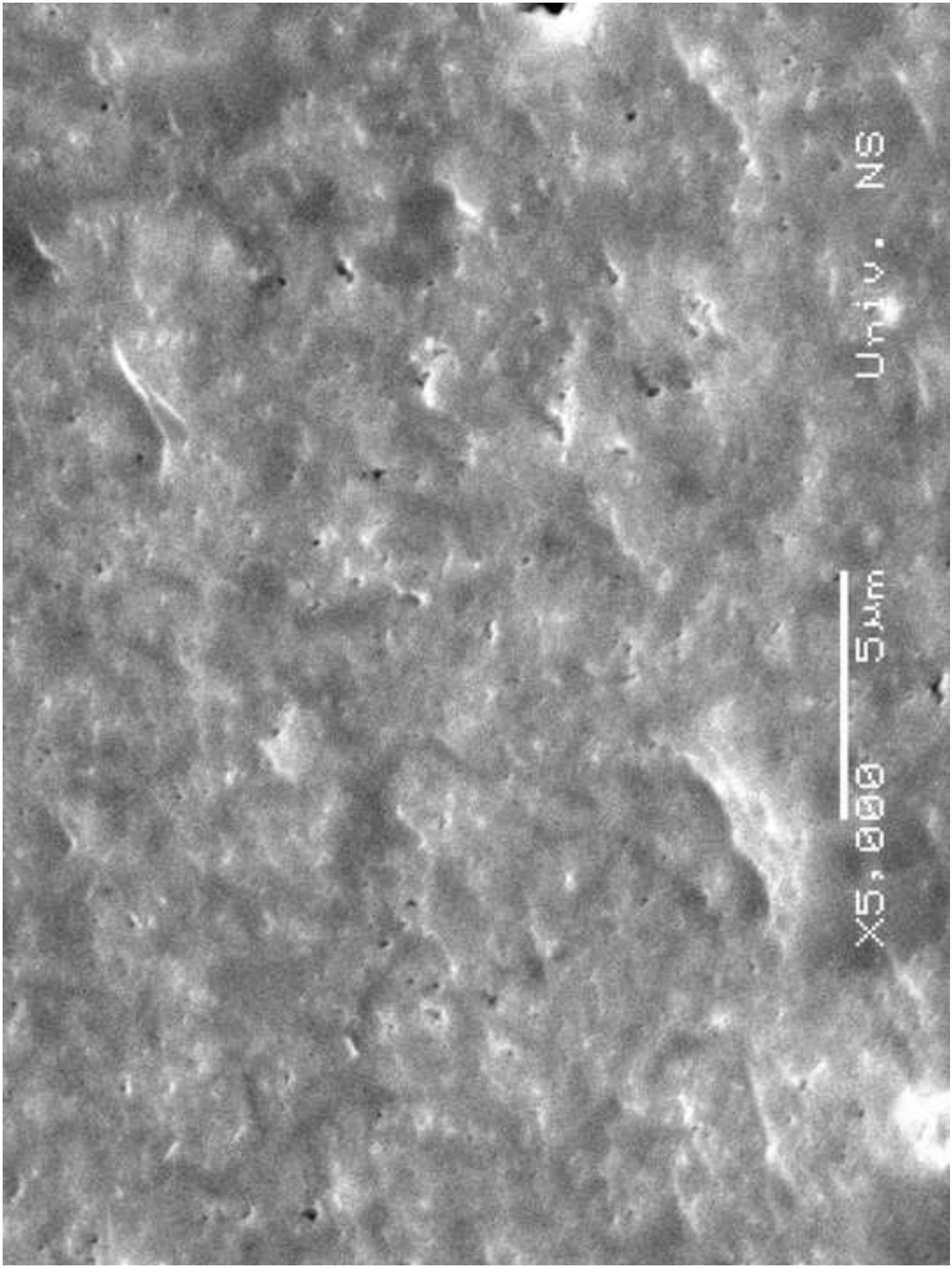

Figure

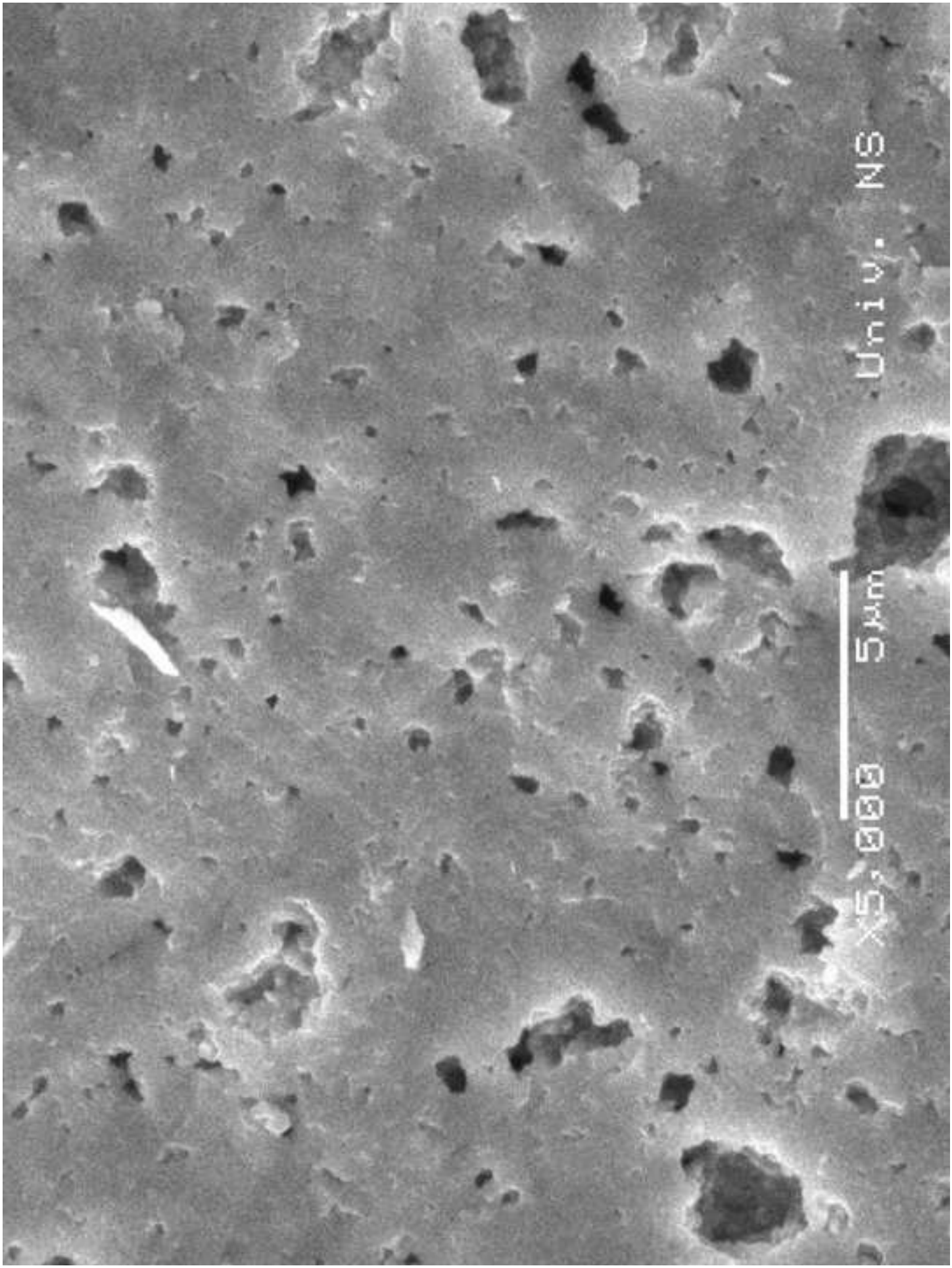

Figure

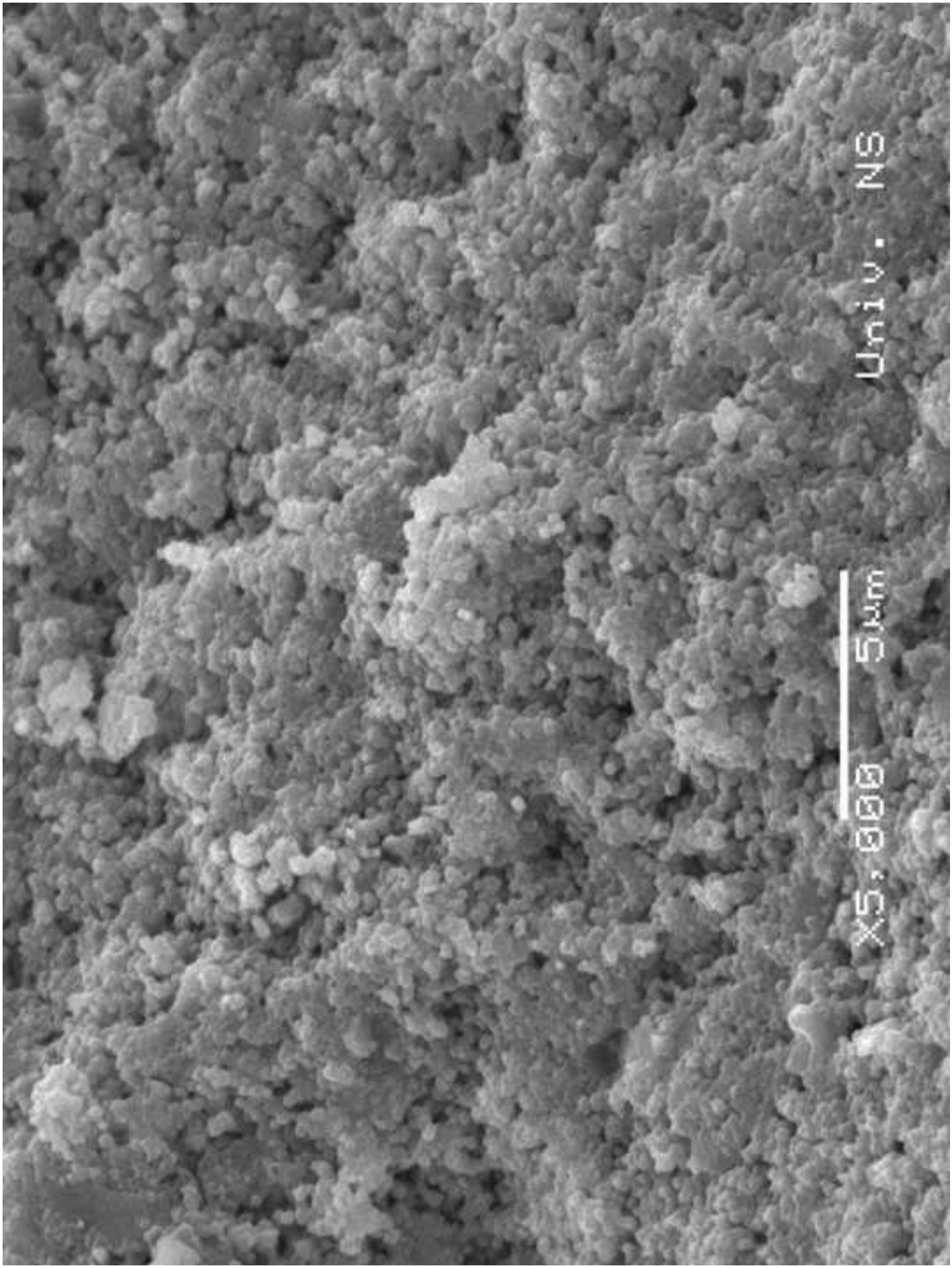

Figure

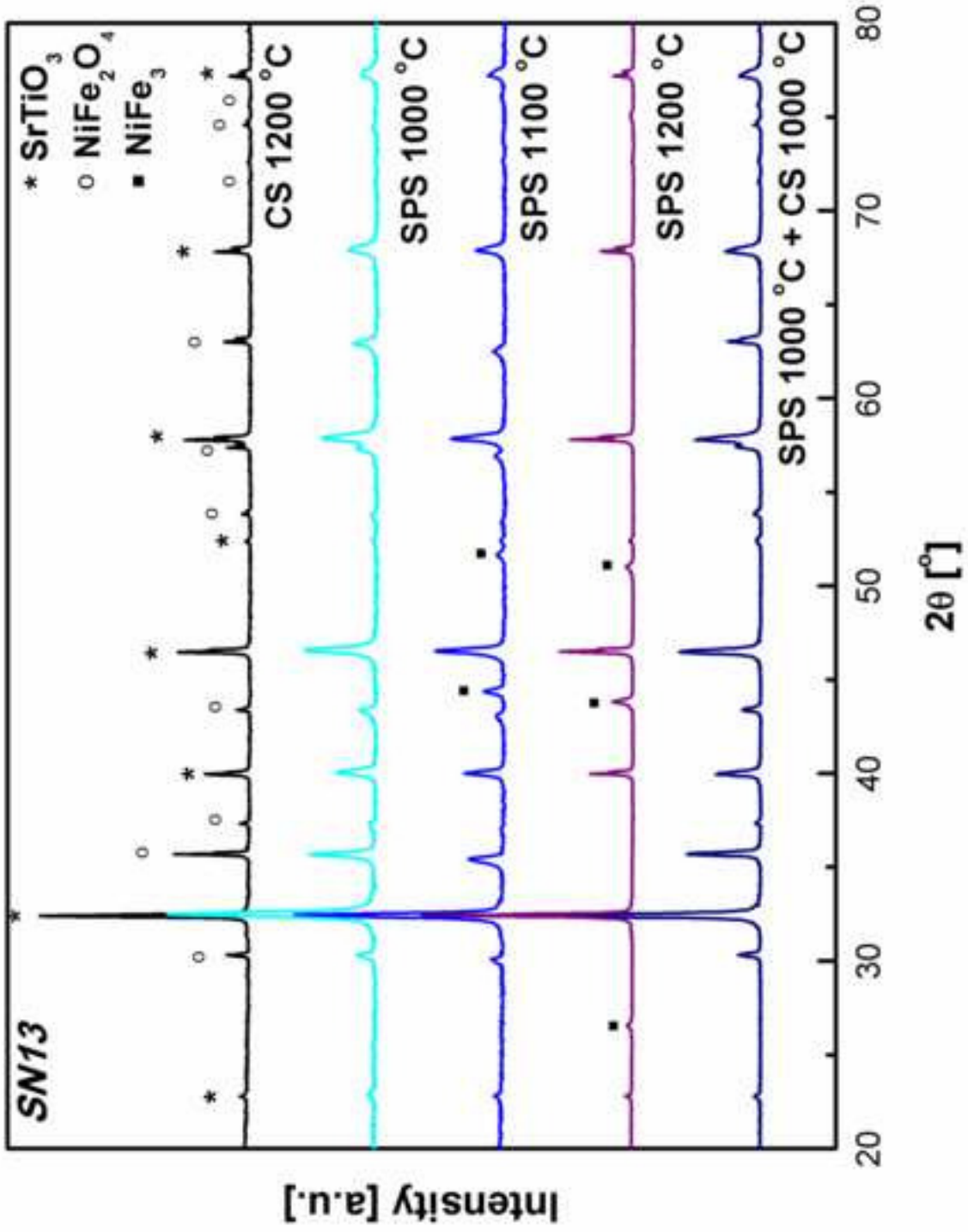
SN13
* SrTiO3
o NiFe2O4
▪ NiFe3
CS 1200 °C
SPS 1000 °C
SPS 1100 °C
SPS 1200 °C
SPS 1000 °C + CS 1000 °C
Intensity [a.u.]
2θ [°]
20
30
40
50
60
70
80

Figure

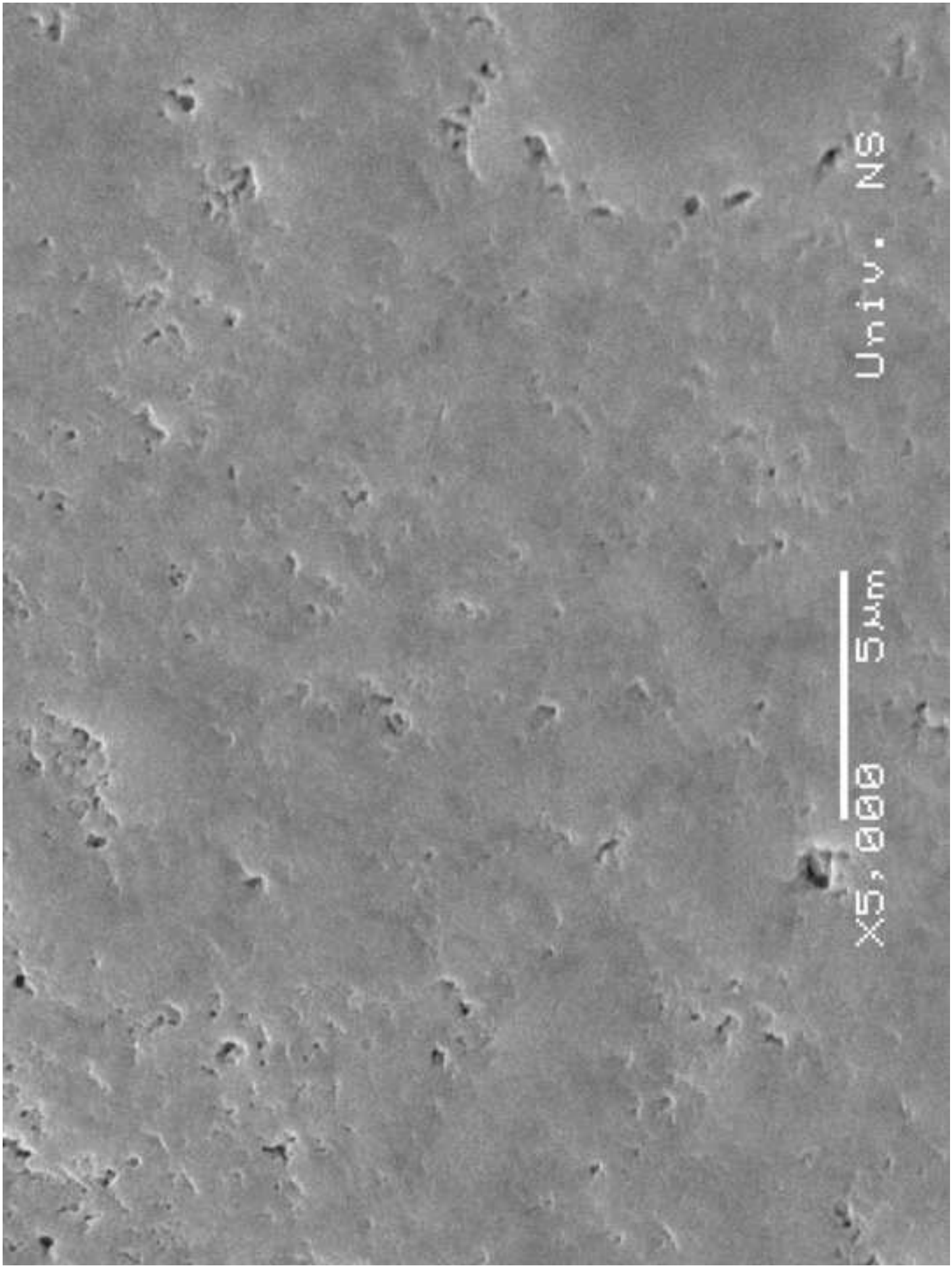

Figure

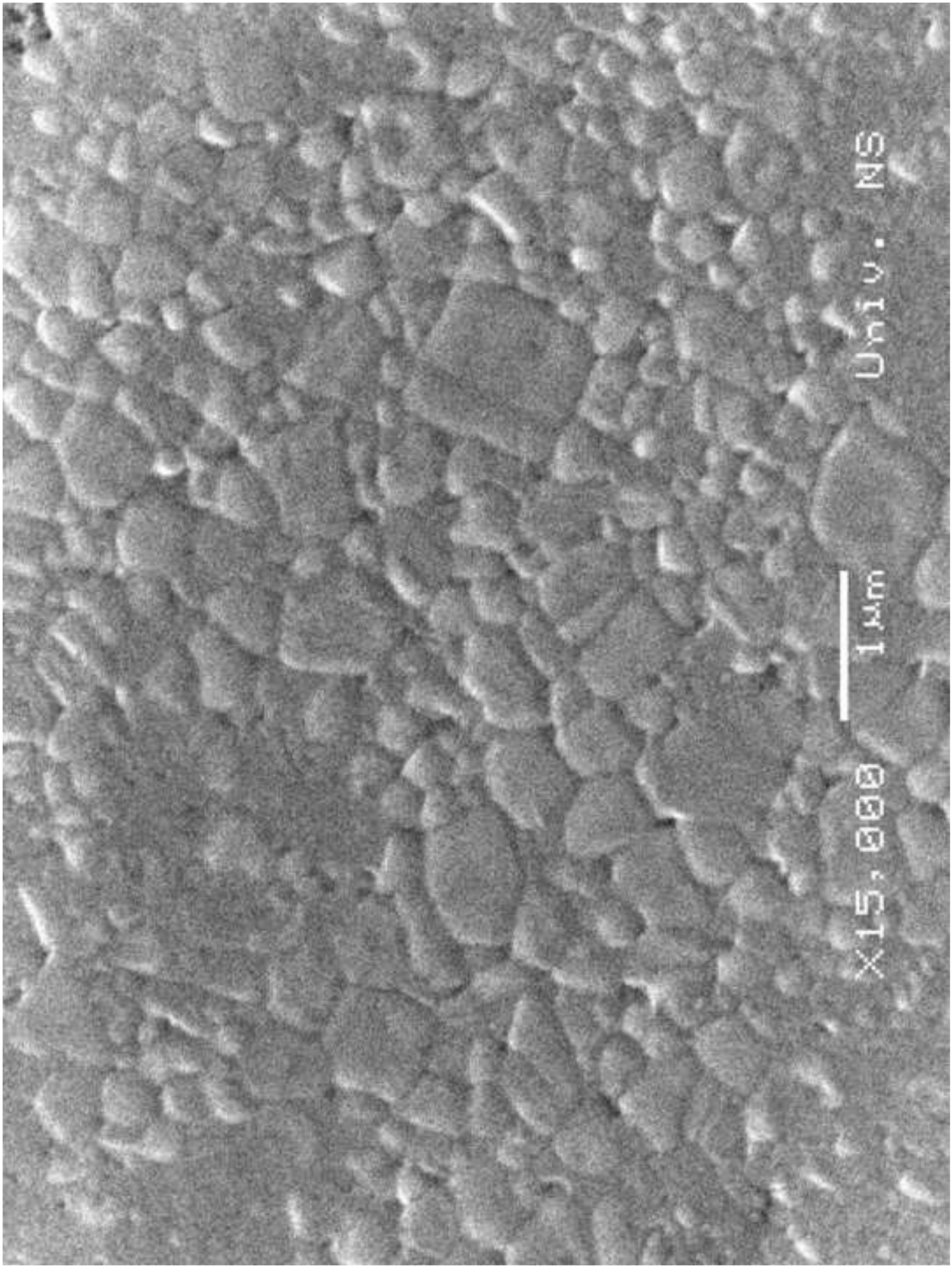

Figure